A study of cloud mixing and evolution using PDF methods. 1. Cloud front propagation and evaporation

Christopher A. Jeffery *
Space and Remote Sensing Sciences (ISR-2), LANL, Los Alamos, NM

Jon M. Reisner
Atmospheric, Climate and Environmental Dynamics (EES-2), LANL, Los Alamos, NM

October 10, 2005

Abstract

The evolution of mean relative humidity (RH) is studied in an isobaric system of clear and cloudy air mixed by an incompressible velocity field. A constant droplet radius assumption is employed that implies a simple dependence of the mixing time-scale, τ_{eddy}, and the reaction (evaporation) time-scale, τ_{react}, on the specifics of the droplet size spectrum. A dilemma is found in the RH e-folding time, τ_{efold}, predicted by two common microphysical schemes: models that resolve supersaturation and ignore subgrid correlations which gives $\tau_{\mathrm{efold}} \sim \tau_{\mathrm{react}}$, and PDF schemes that assume instantaneous evaporation and predict $\tau_{\mathrm{efold}} \sim \tau_{\mathrm{eddy}}$. The resolution of this dilemma, Magnussen and Hjertager (1976)'s EDC model $\tau_{\mathrm{efold}} \sim \max(\tau_{\mathrm{react}}, \tau_{\mathrm{efold}})$, is revealed in the results of 1D eddy-diffusivity simulations and a new PDF approach to cloud mixing and evolution in which evaporation is explicitly resolved and the shape of the PDF is not specified a priori. The EDC model is shown to exactly solve the non-turbulent problem of spurious production of cloud-edge supersaturations described by Stevens et al. (1996), and produce good results in the more general turbulent case.

*Corresponding author address: Christopher A. Jeffery, Los Alamos National Laboratory (ISR-2), PO Box 1663, Mail Stop D-436, Los Alamos, NM 87545, USA. Tel.: (505) 665-9169; fax: (505) 664-0362. Email: cjeffery@lanl.gov

1. Introduction

> It is assumed that an intermittent eddy structure is present in the flow. Liquid and vapour is assumed to be present in a near equilibrium state in certain eddies, while gas and superheated vapour is present in other eddies. Thus the rate of evaporation is limited by the rate of heat and mass transfer between these eddies. [Magnussen and Hjertager (1979, pp. 416)]

The evaporation rate of cloud droplets mixing with entrained air at high turbulent Reynolds numbers is unresolved at the grid-scale of most models, but its accurate prediction is of consequence to the much larger scale issues of cloud radiative forcing (Stephens 2005) and indirect aerosol effects (Lohmann and Feichter 2005). The numerical prediction of subgrid evaporation is typical of a broad class of problems that involve the representation of sub-centimeter-scale microphysical interactions and aerosol transformations at resolution scales of 10 m to 100 km. Rigorous mathematical analysis based on scale-separation can provide new insights (Majda and Souganidis 2000) but its general applicability to dynamic multiscale geophysical phenomena has yet to be determined.

One approach to improve the representation of cloud processes in numerical models involves the diagnosis or prognosis of subgrid moist convection and cloud amount from resolved quantities. A variety of this class of cloud scheme utilizes assumed distributions of subgrid quantities—specified by low-order moments—to provide a self-consistent diagnosis of a variety of in-cloud average and cell-average quantities (Sommeria and Deardorff 1977; Mellor 1977;

Jeffery and Austin 2003). This approach falls under the general moniker of Probability Density Function (PDF) methods.

To date, all implementations of PDF methods in subgrid cloud modeling have employed an "instantaneous" condensation and evaporation (C&E) rate assumption to diagnose liquid water mixing ratio (q_l):

$$q_l \sim \Gamma(q_t - q_s)\{q_t - q_s\} \tag{1}$$

where $\Gamma(y) = \{0, 1\}$ for $\{y < 0, y \geq 0\}$ is a step-function, and total water mixing ratio (q_t) and saturation mixing ratio (q_s) assume a distribution of values in each grid cell. Hereafter, we refer to Eq. (1) as the Instantaneous C&E (InC&E) assumption.

The overall goal of this series of papers is to study cloud mixing and evolution using PDF methods in which (i) turbulent mixing and C&E are explicitly resolved, i.e. the InC&E assumption is relaxed, and (ii) the PDF shape is not specified a priori. In this regard, it is of value to introduce a central theme that will emerge in this series:

> The lack of explicit spatial information in the PDF approach is, simultaneously, both its greatest strength and greatest limitation.

By discarding spatial information, PDF methods avoid the traditional numerical and computational issues that hinder the Eulerian modeling of multiscale systems. But at the same time, PDF evolution equations reveal a new class of statistical quantities—conditional moments—that must be "modeled" and that may depend on implicit spatial structure and evolution.

This article is concerned with the isobaric evaporation rate of cloudy air and its numerical prediction as specified by the evolution of relative humidity (RH). We therefore define *evaporation rate* as the rate of evolution of the mean relative humidity, $\overline{\mathrm{RH}}$, of a grid-cell with internal mixing. The definition of the C&E time-scale, τ_{efold}, follows as the e-folding time of $\overline{\mathrm{RH}}$ evolution.

This work begins with the observation that the evaporation rate predicted by (i) PDF schemes that utilize the InC&E assumption, and (ii) schemes that resolve supersaturation, S, and ignore subgrid correlations, disagree. We refer to this observation as the C&E time-scale dilemma: two common subgrid cloud modeling assumptions, that are in some sense archetypal, are inherently inconsistent. The central thesis of this work is that two distinct modeling approaches (i) 1D eddy-diffusivity modeling and (ii) PDF modeling with resolved mixing and evaporation, both suggest a solution to this dilemma—a solution that is originally due to Magnussen and Hjertager (1976) and that has been independently developed in the combustion literature. Following Magnussen and Hjertager, we refer to the modeling approach that unifies the treatment of cloud evaporation in PDF-based and resolved-S microphysical schemes as the Eddy Dissipation Concept (EDC).

Before proceeding to the outline of this article, it is of value to first introduce the concepts and notation of the PDF approach and the modeling challenges therein. Assuming that droplet radius remains approximately constant during mixing, Reynolds decomposition and averaging gives an equation for $\overline{\mathrm{RH}}$ that contains the correlation $\overline{N'\mathrm{RH}'}$ in the C&E source term where N is droplet concentration, a prime denotes a centered fluctuating quantity, and an overbar denotes a spatial average. In contrast, our development of the PDF equation for RH in Sec. 4a produces the conditional quantity

$$\left\langle N | \widetilde{\mathrm{RH}} = \mathrm{RH} \right\rangle,$$

hereafter $\langle N|\mathrm{RH}\rangle$ for notational convenience, where $\langle \cdot | \widetilde{\mathrm{RH}} = \mathrm{RH} \rangle$ represents a spatial or ensemble average of the random RH field, $\widetilde{\mathrm{RH}}(\boldsymbol{x}, t)$, where the condition $\widetilde{\mathrm{RH}} = \mathrm{RH}$ holds.

Modeling conditional quantities is a formidable challenge but we are guided by boundary conditions in this task. In this work we consider the isobaric mixing of two uniform masses of clear ($\mathrm{RH} = \mathrm{RH}_{\mathrm{env}}$,$N = 0$) and cloudy ($\mathrm{RH} = 1$,$N = \overline{N_c}$) air in the absence of sedimentation and inertial effects. Then parameterization of $\langle N|\mathrm{RH}\rangle$ must obey boundary conditions $\langle N|\mathrm{RH}_{\mathrm{env}}\rangle = 0$, $\langle N|1\rangle = \overline{N_c}$ and normalization

$$\overline{N} \equiv \int \mathcal{P}(\mathrm{RH})\mathrm{dRH}\ \langle N|\mathrm{RH}\rangle,$$

where $\mathcal{P}(\mathrm{RH})\mathrm{dRH}$ is the probability of finding $\widetilde{\mathrm{RH}} \in [\mathrm{RH}, \mathrm{RH} + \mathrm{dRH}]$. These boundary conditions and normalization provides guidance during model development. Once modeled, the conditional quantity $\langle N|\mathrm{RH}\rangle$ influences $\overline{\mathrm{RH}}$ evolution according to

$$\overline{N'\mathrm{RH}'} \equiv \int \mathcal{P}(\mathrm{RH})\mathrm{dRH}\ \left\{\langle N|\mathrm{RH}\rangle - \overline{N}\right\}\mathrm{RH}.$$

This article is organized as follows. In Sec. 2 we consider the isobar mixing of clear and cloudy air in a single grid cell and we derive the evaporation rate predicted by (i) PDF schemes that utilize the InC&E assumption [Sec. 2a] and (ii) microphysics models that resolve S and ignore subgrid correlations [Sec. 2b]. In Sec. 2c we introduce the Damköhler number—the ratio of mixing and reaction (evaporation) time-scales—which facilitates a comparison of PDF and resolved evaporation rates for a

range of atmospheric conditions. In Sec. 3 we study the evaporation rate predicted numerically by a simple 1D eddy-diffusivity model for various initial conditions and diagnosed mixing time-scales; the results of this study are shown to be consistent with Magnussen and Hjertager's EDC model. In Sec. 4 we present a new model of cloud mixing and evaporation based on the evolution of the PDF of RH, and the important role of conditional averaging in this approach is highlighted. In Sec. 5 we test the efficacy of the EDC model in the Stevens et al. (1996) scenario of cloud-front propagation and evaporation; Sec. 6 contains a summary.

2. The C&E time-scale dilemma

In this section we consider the isobar mixing of clear and cloudy air in a single grid cell. The PDF scheme is assumed to describe the grid cell evolution in terms of subgrid fields $\theta_l(\boldsymbol{x},t)$ and $q_t(\boldsymbol{x},t)$, while the resolved scheme that is often employed in LES/CRM models uses $\theta(\boldsymbol{x},t)$ (or equivalently temperature) and $q_v(\boldsymbol{x},t)$. It is often assumed that the LES/CRM subgrid modeling assumption is grid-cell homogeneity, i.e. $\theta = q_v =$ constant (Krueger 1993). However, this assumption is overly restrictive; our approach here is to *formally add* subgrid turbulent mixing and evolution to a single LES/CRM grid cell which retains the symmetry between the PDF and LES/CRM approaches.

2a. *The InC&E assumption and its implications*

Consider, first, the C&E time-scale implied by subgrid PDF schemes that use the InC&E assumption with prognostic equations for the subgrid variance of q_t and liquid water potential temperature, θ_l, in a closed cell. Assume, furthermore, that these prognostic equations predict the evolution of variance without error, i.e. the prediction of the PDF scheme is consistent with the exact evolution of the subgrid fields $\{\theta_l(\boldsymbol{x},t), q_t(\boldsymbol{x},t)\}$. Then beginning with advection-diffusion equations for $\{\theta, q_v\}$, assuming molecular diffusion of q_l, linearizing fluctuations of q_s^{-1} and $q_s(T)$ about the mean and introducing a molecular diffusivity, $\kappa \geq 0$ (assumed equal for q_v and θ) leads to an equation for the variance of RH_t, $\mathrm{var}(\mathrm{RH}_t)$:

$$\begin{aligned} \frac{\partial \mathrm{var}(\mathrm{RH}_t)}{\partial t} &= -2\chi \\ \chi &\equiv \kappa \overline{|\boldsymbol{\nabla}\mathrm{RH}_t|^2}, \end{aligned} \tag{2}$$

where $\mathrm{RH}_t = q_t/q_s$, overbar denotes a spatial average and χ is the scalar dissipation rate† Equation (2) illustrates the key dynamical features of subgrid PDF schemes that utilize the InC&E assumption, namely, $\mathrm{var}(\mathrm{RH}_t)$ decays to zero with a turbulent mixing time-scale

$$\tau_{\mathrm{eddy}} \equiv \mathrm{var}(\mathrm{RH}_t)/\chi,$$

that is unresolved and must be modeled. Thus the evaporation rate is largely determined by τ_{eddy} and is independent of the microscopic phase-change (reaction) time-scale, τ_{react}, which is assumed zero in the InC&E limit.

We are thus led to the following conclusion:

> The evaporation rate of unmixed clear and cloudy air predicted by a PDF scheme and the InC&E assumption in a grid cell with internal unresolved divergenceless advective-diffusive mixing depends on τ_{eddy} and is independent of τ_{react}.

2b. *Resolved evaporation rates and the C&E dilemma*

High resolution cloud models, e.g. Large Eddy Simulation (LES) of clouds, and somewhat coarser resolution Cloud Resolving Models (CRMs), often explicitly resolve τ_{react}. While it is typically assumed that LES/CRM assume subgrid homogeneity, we relax this assumption here and consider an isobaric model grid cell, mixed by internal velocity $\boldsymbol{u}$ and molecular diffusivity κ, that has an externally specified intra-cell flux, $\boldsymbol{\Phi}_{\mathrm{flux}}$, and is otherwise closed, i.e. $\boldsymbol{\nabla}\mathrm{RH} = \boldsymbol{u} = 0$ on cell faces.

$$\begin{aligned} \frac{\partial \mathrm{RH}}{\partial t} + \boldsymbol{u}\cdot\boldsymbol{\nabla}\mathrm{RH} &= -\boldsymbol{\nabla}\cdot\boldsymbol{\Phi}_{\mathrm{flux}} + \kappa\nabla^2\mathrm{RH} + \frac{1-\mathrm{RH}}{\tau_{\mathrm{react}}} \\ \tau_{\mathrm{react}}(\boldsymbol{x},t) &\equiv \frac{1}{4\pi D_v N}\frac{r+a}{r^2}, \end{aligned} \tag{3}$$

where D_v is the (assumed constant) diffusivity of water vapor, a is an accommodation length introduced for analytic convenience and the small temperature dependence of τ_{react} has been ignored.

The time-scale τ_{react} was first introduced by Squires (1952) and termed the phase relaxation time. It plays a central role in the results of Wang et al. (2003).† Wang et al. argue that the effective time-scale over which turbulence mixing can affect the cloud liquid water flux is $(1/\tau_{\mathrm{react}} + 1/\tau_{\mathrm{R}})^{-1}$ (Wang et al. 2003, pp. 270) where τ_{R} is the cloud-scale large-eddy turnover time and should not be confused with the subgrid mixing time τ_{eddy}.

The behavior described by Wang et al. is consistent with all current models that resolve RH and

†For analytic convenience we defi ne χ as the dissipation rate of half variance. Note that Eqs. (2) and (3) both assume temperature fluctuations $T' \ll R_v\overline{T}^2/L_v$.

†Note that ρ_l is non-dimensional (water density divided by air density) in Eq. (18) of Wang et al. (2003)

ignore subgrid correlations as the following proof demonstrates. We first note that these cloud parameterizations replace the subgrid spatio-temporal field $\tau_{\rm react}(\boldsymbol{x},t)$ with its grid cell average $\overline{\tau_{\rm react}}(t)$—an assumption that is less restrictive than assuming subgrid homogeneity. Averaging Eq. (3) with this assumption and solving the resulting ODE gives the longtime behavior

$$\overline{\rm RH}(t) = \int^t {\rm d}\xi\ \exp\left[-\int_\xi^t {\rm d}\xi'\ \overline{\tau_{\rm react}}^{-1}(\xi')\right] \left\{\frac{1}{\overline{\tau_{\rm react}}(\xi)} - \frac{1}{V}\int {\rm d}\boldsymbol{\lambda}\ \hat{\boldsymbol{x}}\cdot\boldsymbol{\Phi}_{\rm flux}(\boldsymbol{\lambda},\xi)\right\} \quad (4)$$

where V is the grid cell volume, $\int {\rm d}\boldsymbol{\lambda}$ is a surface integral over cell faces and $\hat{\boldsymbol{x}}$ is a unit-vector normal to the cell face at $\boldsymbol{\lambda}$.

Eq. (4) is a function of two distinct time-scales: $\overline{\tau_{\rm react}}$ (t) and the grid-scale time, $\tau_{\rm R}$, associated with $\boldsymbol{\Phi}_{\rm flux}$. Inspection of Eq. (4) reveals that the ${\rm RH}$ "evolution rate" predicted by the subgrid assumption $\tau_{\rm react}(\boldsymbol{x},t)\rightarrow\overline{\tau_{\rm react}}(t)$ is consistent with Wang et al.'s response time $(1/\overline{\tau_{\rm react}}+1/\tau_{\rm R})^{-1}$. Of central importance, the evaporation rate predicted by Eq. (4) is given solely by $\overline{\tau_{\rm react}}$; the subgrid mixing time associated with advective-diffusive mixing, i.e. $\boldsymbol{u}$ and κ, does not appear in (4). Also, since (4) is independent of the variability in the subgrid RH field it follows that the assumption of subgrid homogeneity is a special case of this more general result. It must be emphasized that the independence of evaporation (reaction) rate and κ implied by Eq. (4) is specific to advective-diffusive reaction that is linear combined with $\tau_{\rm react}(\boldsymbol{x},t)\rightarrow\overline{\tau_{\rm react}}(t)$; reaction rates for explicitly non-linear reactions will always depend on κ, regardless of the subgrid modeling assumptions employed.

The above results lead us to the following conclusion:

> The evaporation rate of unmixed clear and cloudy air predicted by current S-resolving microphysical schemes in a grid cell with internal unresolved divergenceless advective-diffusive mixing depends on $\tau_{\rm react}$ and is independent of $\tau_{\rm eddy}$.

This statement contradicts the conclusion of Sec. 2a. Moreover, it reveals the following dilemma. Both the InC&E assumption—as its name implies—and the resolved-S model of evaporation in the limit $\tau_{\rm react}\rightarrow 0$ are considered to converge to the "fast reaction" limit of divergenceless advective-diffusive evaporation. Yet these two models predict different evaporation rates in this limit. This is what we refer to as the C&E time-scale dilemma: two common subgrid cloud modeling assumptions, that are in some sense archetypal, are inherently inconsistent.

2c. *Damköhler number*

Of central importance in this work is the Damköhler number (Damköhler 1940)

$${\rm D_a} = \frac{\text{mixing time-scale}}{\text{reaction time-scale}},$$

which provides insight into the fundamental nature of mixing and evaporation in clouds. In what follows we choose to define ${\rm D_a}$ in terms of the in-cloud number concentration

$${\rm D_a} = 4\pi D_v \overline{N_c}\frac{r^2}{r+a}\tau_{\rm eddy}, \quad (5)$$

where $\overline{N_c}$ is the cloud-averaged (as opposed to grid-averaged) number concentration. This definition of reaction time-scale differs from $\overline{\tau_{\rm react}}$ which involves the grid-averaged concentration, $\overline{N}$, but is advantageous because $\overline{N_c}$ is often measured experimentally and is more easily estimated. An estimation of the range of ${\rm D_a}$ as defined in Eq. (5) provides insight into relative differences in evaporation rate predicted by PDF and resolved-S models.

Two contour plots of ${\rm D_a}$ are shown in Fig. 1 where standard Kolmogorov scaling provides the estimate, $\tau_{\rm eddy}=0.1\varepsilon^{-1/3}L^{2/3}$ with L the grid cell length and ε the kinetic energy dissipation rate. The plots indicate that ${\rm D_a}$ spans four orders of magnitude in the range 10^{-2} to 10^2 for a broad range of $\{L,\overline{N_c},r\}$ values and $\varepsilon=0.01\ {\rm m^2\ s^{-3}}$. In particular, an indirect aerosol effect is observed with ${\rm D_a}$ increasing linearly with N at fixed r ($N^{2/3}$ at fixed q_l) as indicated by Eq. (5). The contour ${\rm D_a}=1$—where we expect the PDF and resolved models to predict similar evaporation rates for small $\phi_{\rm sub}$—tends to run through a relatively narrow range of droplet sizes between 2 and 10 $\mu{\rm m}$. For small drops $r\ll 2\ \mu{\rm m}$ the InC&E assumption predicts greater evaporation rates than resolved-S schemes while for large drops $r\gg 10\ um$ the resolved model predicts faster evaporation than the InC&E approach. Taken as a whole, Fig. 1 reiterates the seriousness of the C&E time-scale dilemma: evaporation rates predicted by subgrid PDF schemes that use the InC&E assumption and LES/CRM models that resolve S and ignore subgrid correlations may vary more than two orders of magnitude for realistic atmospheric conditions.

3. Cloud front evaporation: Eddy-diffusivity model

In this section we investigate cloud front propagation and evaporation in a closed cell using a simple one-dimensional eddy-diffusivity model. A distinguishing

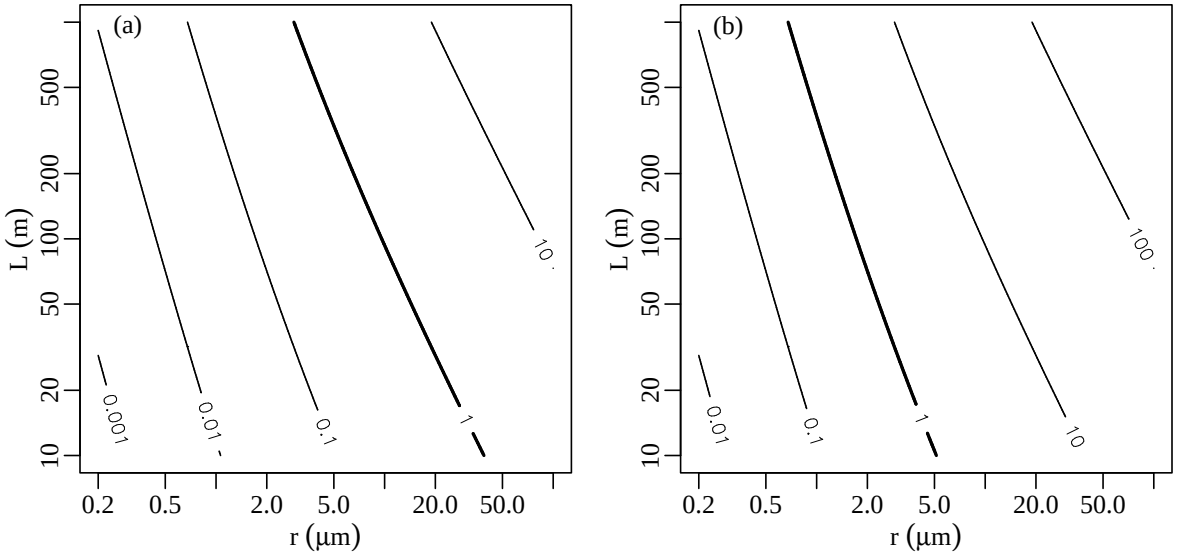

Figure 1: Contour plots of $\mathrm{D_a}$ as a function of $\{r, L\}$ for $N_c = 50\ \mathrm{cm}^{-3}$ [Fig. 1(a)] and $N_c = 500\ \mathrm{cm}^{-3}$ [1(b)], typical of clean marine and polluted marine/continental environments, respectively (Heymsfield and McFarquhar 2001). $\mathrm{D_a}$ is computed with Eq. (5), the Kolmogorov estimate $\tau_{\mathrm{eddy}} = 0.1\varepsilon^{-1/3}L^{2/3}$ and $\varepsilon = 0.01\ \mathrm{m}^2\ \mathrm{s}^{-3}$. The figures reveal that a range of $\mathrm{D_a}$ values between 10^{-2} and 10^2 exist for typical atmospheric conditions and model grid sizes.

feature of our cloud model is the assumption that droplet radius is time-independent. Although this assumption does not strictly conserve liquid water, it is appropriate for $\mathrm{RH}_t > 1$, large drops and small subsaturations. The advantage of the constant radius assumption is that it leads to cloud front dynamics that are independent of the specifics of the droplet size distribution.

3a. *Cloud model*

The cloud model of interest is given by the following coupled PDEs:

$$\begin{aligned} \frac{\partial \mathrm{RH}}{\partial t} &= \kappa_e \nabla^2 \mathrm{RH} + \epsilon N(1 - \mathrm{RH}) \\ \frac{\partial N}{\partial t} &= \kappa_e \nabla^2 N, \end{aligned} \tag{6}$$

with $\nabla \mathrm{RH} = \nabla N = 0$ on the system boundaries, $\kappa_e \geq 0$ an eddy-diffusivity and $\epsilon \geq 0$ a constant. The C&E source term in the RH equation follows from Eq. (3) using the time-independent droplet radius approximation $r(\boldsymbol{x}, t) = \mathrm{constant}$. Following Grabowski (1993) and Majda and Souganidis (2000) we assume that the cloud ($\mathrm{RH} = 1, N > 0$) and environmental air ($\mathrm{RH} < 1, N = 0$) initially occupy disjoint regions of space. Of course, the constant droplet radius assumption implies the asymptotic $\mathrm{RH}(\boldsymbol{x}, t) \to 1$ as $t \to \infty$.

We consider two different sets of initial conditions: 1_Front simulations in which the system is divided into two adjacent regions of clear and cloudy air and 2_Front simulations with two equal-sized regions of cloudy air surrounding a region of clear air. As the names imply, 1_Front simulations exhibit a single front of cloudy air propagating across the system while two such fronts exist for 2_Front initial conditions. The initial system fraction of clear (cloudy) air is denoted by ϕ_{sub} (1-ϕ_{sub}). Following the introduction and discussion of Damköhler number in Sec. 2b we find $\mathrm{D_a} = \epsilon \overline{N_c} \tau_{\mathrm{eddy}}$ for Eqs. (6) with $\overline{N_c} = \overline{N}(1 - \phi_{\mathrm{sub}})^{-1}$ such that $\tau_{\mathrm{react}}/\tau_{\mathrm{eddy}} = (1 - \phi_{\mathrm{sub}})^{-1}\mathrm{D_a}^{-1}$.

3b. *Model predictions using* $\tau_{\mathrm{eddy}} \sim L^2/\kappa_e$

A comparison of the RH e-folding time, τ_{efold}, predicted by Eqs. (6) is shown in Fig. 2 for $\phi_{\mathrm{sub}} \in [0.05, 0.95]$. In this comparison the mixing time-scale is taken as $\tau_{\mathrm{eddy}} \sim L^2/\kappa_e$ where L is the size of the system domain. This definition of τ_{eddy} is consistent with the subgrid large-eddy turn-over time.

Figure 2 depicts two distinct regimes of evaporative behavior. For small $(1 - \phi_{\mathrm{sub}})\mathrm{D_a}$ [upper right corner], mixing occurs much faster than evaporation and $\tau_{\mathrm{efold}} = \tau_{\mathrm{react}}$ independent of τ_{eddy}. This

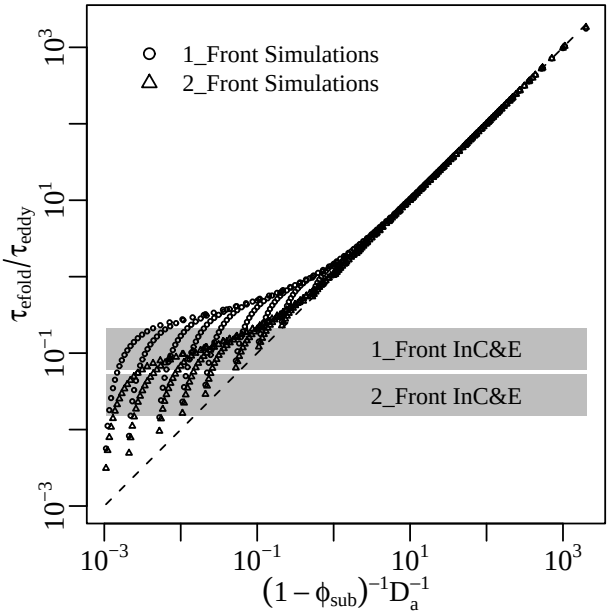

Figure 2: Plot of $\tau_{\rm efold}/\tau_{\rm eddy}$ as a function of $(1-\phi_{\rm sub})^{-1}{\rm D_a}^{-1} = \tau_{\rm react}/\tau_{\rm eddy}$ predicted by Eqs. (6) with $\tau_{\rm eddy} = 0.1L^2/\kappa_e$. Each "finger" in the lower left corner represent 21 different $\phi_{\rm sub}$ values at fixed ${\rm D_a}$ with $\phi_{\rm sub} \in [0.05, 0.95]$. The fingers are not visible in the upper right corner where rapid mixing implies $\tau_{\rm efold} = \tau_{\rm react}$ independent of $\phi_{\rm sub}$.

is the high-resolution limit where the approximation $\tau_{\rm react}(\boldsymbol{x}, t) = \overline{\tau_{\rm react}}(t)$ is valid since the system is well-mixed for $t \gg \tau_{\rm eddy}$. In contrast, for large $(1-\phi_{\rm sub}){\rm D_a}$ [lower left corner] evaporation occurs faster than mixing and $\tau_{\rm efold}$ appears to cluster in the range $\{0.01, 1\}$ $\tau_{\rm eddy}$ independent of $\tau_{\rm react}$. This is consistent with the behavior of subgrid PDF methods that use the InC&E assumption. We also find that $\tau_{\rm efold}$ for the 2_Front simulations is persistently smaller at large ${\rm D_a}$ than the 1_Front $\tau_{\rm efold}$ for a given $\{{\rm D_a}, \phi_{\rm sub}\}$. This behavior is expected since the 2_Front simulations have—as their name implies—approximately twice the interfacial area between clear and cloudy air for evaporation to occur.

To help clarify the relationship between predictions of the resolved-S and InC&E models and the behavior of Eqs. (6), the predictions of these models are also shown in Fig. 2. The $\tau_{\rm efold}$ predicted by resolved schemes is simply the 1-to-1 line (dashed) in the figure. It is more difficult to determine $\tau_{\rm efold}$ predicted by the InC&E assumption since Eqs. (6) do not strictly conserve q_t. However, assuming that the constant radius approximation is consistent with a net change in q_l between 1 and 30% ($\Delta \ln r \in [0.003, 0.112]$) and integrating over $\phi_{\rm sub}$ gives the two shaded regions in Fig. 2 as described in Appendix A. These additional comparisons reiterate that $\tau_{\rm efold}$ predicted by Eqs. (6) is consistent with typical LES/CRM models for $(1-\phi_{\rm sub}){\rm D_a} < 1$ and the InC&E assumption for $(1-\phi_{\rm sub}){\rm D_a} > 1$, and inconsistent otherwise.

3c. *Model predictions using* $\tau_{\rm eddy} \sim {\rm var(RH)}/\chi$

Inspection of Fig. 2 reveals an unsatisfactory aspect of the simulation results. Namely, $\tau_{\rm efold}$ appears to exhibit a strong dependency on initial conditions, i.e. 1_Front vs 2_Front, for a given $\phi_{\rm sub}$. These subgrid initial conditions are, in general, unknown.

Motivated by the discussion of the InC&E assumption in Sec. 2a we introduce the mixing time-scale

$$\tau_{\rm eddy} = \frac{1}{\tau_{\rm efold}} \int_0^{\tau_{\rm efold}} {\rm d}t \, \frac{{\rm var(RH)}}{\chi}, \qquad (7)$$

with scalar dissipation rate $\chi = \kappa_e \overline{|\boldsymbol{\nabla} {\rm RH}|^2}$; Eq. (7) describes a time-averaged measure of the rate of ${\rm RH}$ variance erosion during advective-diffusive mixing. C&E time-scales for $\phi_{\rm sub} \in [0.05, 0.95]$ are shown in Fig. 3 with $\tau_{\rm eddy}$ given by Eq. (7).

Comparison of Figs. 2 and 3 reveals that ${\rm var(RH)}/\chi$ is a much more genuine measure of scalar mixing time than L^2/κ_e. Indeed, this should come as no surprise since χ is an essential quantity in the Oboukhov–Corrsin theory of turbulent advective-diffusive mixing (Tennekes and Lumley 1972, Chap. 8). However, it should be emphasized that Fig. 3 does *not* imply that $\tau_{\rm efold}$ is independent of initial conditions. Rather, given a modeled or observed cloud-clear air interface that is complex and potentially self-similar (fractal), Fig. 3 reveals that just two well-defined statistical quantities—χ and ${\rm var(RH)}$—form the foundation of the relationship between $\tau_{\rm eddy}$ and the resolved (or observed) features of the interface.

3d. *The Eddy Dissipation Concept (EDC) model*

The results of Fig. 3 can be quantified, to first approximation, by the simple expression

$$\tau_{\rm efold} = \max\{0.35\tau_{\rm eddy}, \tau_{\rm react}\}, \qquad (8)$$

with $\tau_{\rm eddy}$ given by Eq. (7). Equation (8) is also valid—but less accurate—for $\tau_{\rm eddy} \sim L^2/\kappa_e$.

Equation (8) resolves the C&E time-scale dilemma described in Sec. 2b. Neither $\tau_{\rm eddy}$ predicted by resolved-S schemes nor the InC&E assumption are uniformly valid. Rather, the resolved model is valid

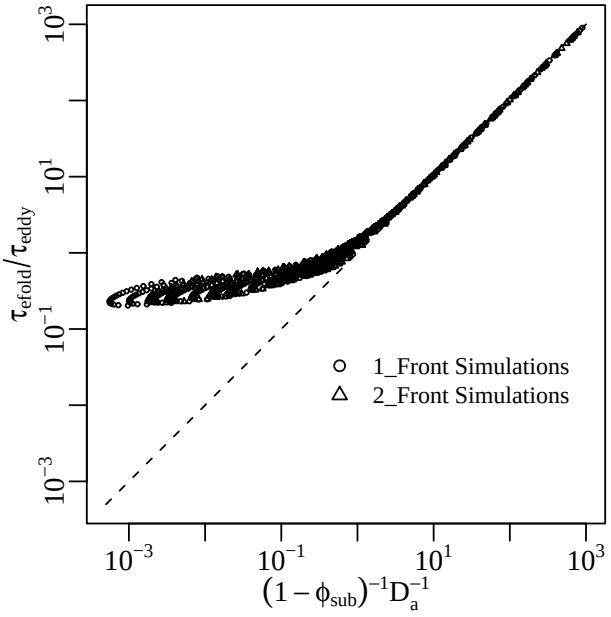

Figure 3: Plot of $\tau_{\rm efold}/\tau_{\rm eddy}$ as a function of $(1-\phi_{\rm sub})^{-1}{\rm D_a}^{-1}$ predicted by Eqs. (6) with $\tau_{\rm eddy}$ given by Eq. (7). Comparison of Fig. 2 and 3 reveals that the diagnosis of $\tau_{\rm eddy}$ from χ provides a superior estimate than $\tau_{\rm eddy} \sim L^2/\kappa_e$.

for $(1-\phi_{\rm sub}){\rm D_a} < 1$ and the InC&E assumption for $(1-\phi_{\rm sub}){\rm D_a} > 1$.

Equation (8), albeit unexplored by the cloud physics community, is not new. In the combustion community, Eq. (8) is typically referred to as the Eddy Dissipation Concept (EDC) model. It is due to Magnussen and Hjertager (1976) who originally used $\tau_{\rm eddy} \sim K/\varepsilon$ where K is kinetic energy. A variant of Eq. (8) was suggested earlier by Spalding (1971). The important role of χ in the evaluation of $\tau_{\rm eddy}$ was first emphasized by Bilger (1976) in the fast chemistry limit, ${\rm D_a} \to \infty$.

A quotation from Magnussen and Hjertager (1979), reproduced at the start of this article, provides a physical interpretation of EDC for the turbulent evolution of a two-phase (liquid-vapor) mixture injected into a hot gas stream at large ${\rm D_a}$. Magnussen and Hjertager recognize that when the liquid-vapor mixture comes into contact with the hot gas, the liquid will rapidly evaporate ($\tau_{\rm react} \to 0$). They conclude that the net evaporation rate *for the system* ($\tau_{\rm efold}$) is therefore controlled by the rate at which the liquid-vapor mixes into the hot stream ($\tau_{\rm eddy}$). This is the fundamental nature of reactive advective-diffusive mixing at large ${\rm D_a}$ for the class of non-linear reaction types that includes C&E.

3e. *EDC, Broadwell–Breidenthal and reaction type*

The phenomenological model of Broadwell and Breidenthal (1982) is based on the reaction type $A + B \stackrel{k}{\to} C$ with reaction rate k, where the scalar mixing statics, e.g. the surface area per unit volume of interface between the two reactants, are assumed k-independent. In contrast, mixing of cloudy and clear air with $\overline{\rm RH_t} > 1$ is consistent with the reaction type $A + B \stackrel{k}{\to} B$ where A (B) represents subsaturated (saturated) air, respectively. In this case, the scalar mixing statics are strongly k-dependent at large ${\rm D_a}$ because a faster evaporation rate enhances the ${\rm RH}$ gradients across the cloud front which, in turn, affects the statistics of the (centimeter-scale) filaments where evaporation is occurring. This cloud-front sharpening is revealed in the cumulative probability density function (${\rm CDF}$) that ${\rm RH_{env}} + \epsilon < {\rm RH} < 1 - \epsilon$ with $0 < \epsilon \ll 1 - {\rm RH_{env}}$ which is a measure of the volume fraction of ${\rm RH}$-filaments when $\nabla\kappa_e = 0$.

A plot of the ${\rm CDF}$ averaged over $\tau_{\rm efold}$ is shown in Fig. 4 for the simulations of Sec. 3c and $\epsilon = 0.01(1 - {\rm RH_{env}})$. As in Fig. 3, two distinct regimes are evident in the small and large ${\rm D_a}$ limits. For small $(1-\phi_{\rm sub}){\rm D_a}$, the average system state is well-mixed and hence the "filament" where evaporation is occuring is the entire system volume. In contrast, at large $(1-\phi_{\rm sub}){\rm D_a}$ the front sharpening process decreases the volume fraction of filaments with increasing ${\rm D_a}$. This behavior—valid for $\overline{\rm RH_t} > 1$—contradicts the Broadwell–Breidenthal model where the filament statistics are assumed to be independent of $\tau_{\rm react}$, and hence ${\rm D_a}$.

Unfortunately, Fig. 4 also reveals a deficiency of the simple 1D eddy-diffusivity model used in this section: the filament volume fraction scatters widely and, moreover, is too high at large ${\rm D_a}$. This over-prediction of filament volume fraction is not unexpected; the tendency of eddy-diffusion to predict a turbulent transport that is too smooth and overly diffusive is well known. A new PDF model of cloud mixing is introduced in Sec. 4 that corrects this deficiency.

3f. *EDC and Reynolds decompositions*

To conclude this section, it is of interest to recast the subgrid approximation $\tau_{\rm react}(\boldsymbol{x},t) = \overline{\tau_{\rm react}}(t)$ of Sec. 2b in terms of a Reynolds decomposition of subgrid quantities (Cooper 1989; Stevens et al. 1998). Denoting centered fluctuating variables with a prime, this approximation is rewritten $\overline{S'\tau_{\rm react}{}'} = 0$, in general, or $\overline{N'S'} = 0$ for the constant radius approxima-

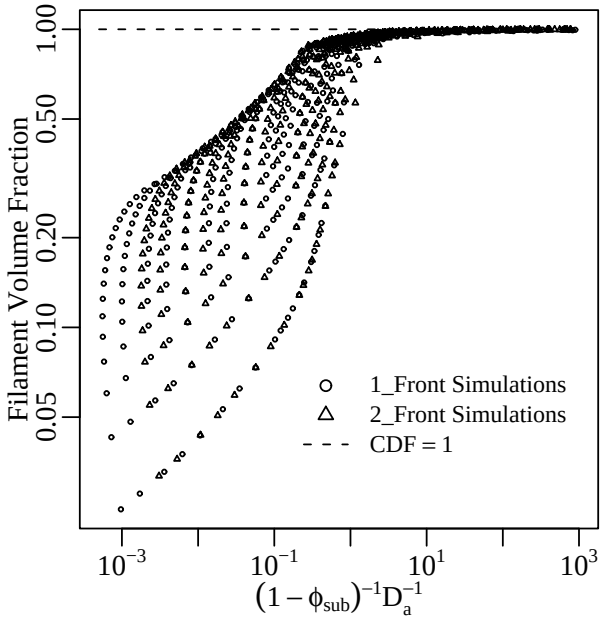

Figure 4: Plot of the cumulative probability that $\mathrm{RH}_{\mathrm{env}} + \epsilon < \mathrm{RH} < 1 - \epsilon$, averaged over τ_{efold} and predicted by the 1_Front and 2_Front simulations of Sec. 3c with $\epsilon = 0.01(1 - \mathrm{RH}_{\mathrm{env}})$. The figure shows increasing RH-front sharpening with increasing $\mathrm{D_a}$.

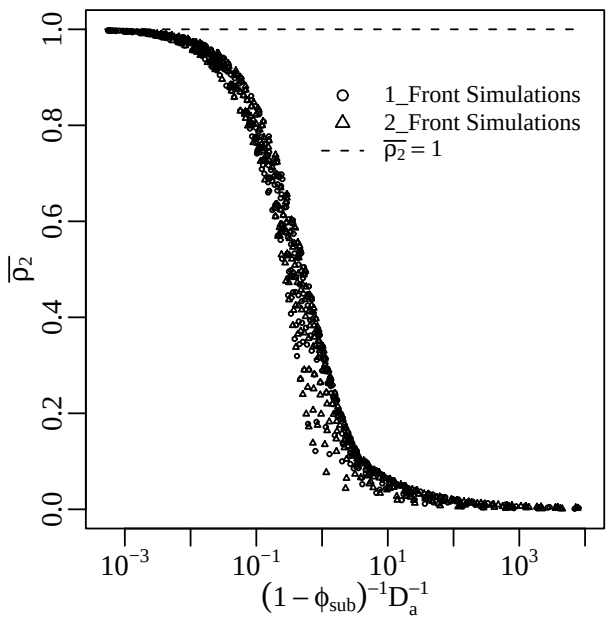

Figure 5: Plot of the correlation coefficient, $\rho_2 = \overline{N'S'}/(\overline{N}\overline{|S|})$, averaged over τ_{efold} and predicted by the 1_Front and 2_Front simulations of Sec. 3c. The correlation $\overline{N'S'}$ appears in the evolution equation for $\overline{\mathrm{RH}}$ and acts to increase τ_{efold} at large $\mathrm{D_a}$.

tion considered here.

There are two normalizing coefficients of interest, $c \in \{c_1, c_2\}$, such that $c\overline{N'S'}$ is non-dimensional. The first, $c_1 = (\sigma_N \sigma_S)^{-1}$ gives the standard correlation coefficient $\rho_1 \in [-1, 1]$ where σ_X is the standard deviation of quantity X. Not surprisingly, N and S are highly correlated with $\rho_1 \approx 1$ independent of $\mathrm{D_a}$ (not shown). The second coefficient, $c_2 = (\overline{N}\overline{|S|})^{-1}$ provides a correlation coefficient ρ_2 that is a measure of the relative importance of the covariance $\overline{N'S'}$. In particular, $\rho_2(t = 0) = 1$ for the "cloud-front" initial conditions used in this section and $\rho_2(t \to \infty) = 0$ for the well-mixed final state.

A plot of ρ_2 averaged over τ_{efold} is shown in Fig. 5 for the simulations of Sec. 3c. The results of this figure are consistent with and compliment the results of Fig. 3. For $(1-\phi_{\mathrm{sub}})\mathrm{D_a} > 1$, $\overline{N'S'}$ is of relative importance (Fig. 5) and neglect of this covariance leads to a dramatic underestimation of τ_{efold} (Fig. 3). This behavior reiterates that LES/CRM models which resolve S and assume $\overline{N'S'} = 0$ overestimate evaporation at large $\mathrm{D_a}$.

4. Cloud front evaporation: PDF model

The simple 1D eddy-diffusivity model of cloud front propagation and evaporation introduced in Sec. 3 reveals a C&E phenomenlogy with distinct small and large Damköhler number limits, in agreement with the EDC model introduced three decades ago by Magnussen and Hjertager. Yet, a fundamental objection to this simple modeling approach can be raised: eddy-diffusion is a mean-field (i.e. ensemble averaged) model of turbulent transport that should not be expected to hold in the large $\mathrm{D_a}$ limit where front-sharpening leads to steep gradients and possibly "non-diffusive" transport and behavior. Thus the consistency of EDC and non-diffusive front sharpening with increasing $\mathrm{D_a}$ has yet to be established.

In this section we introduce a new class of cloud modeling based on PDF methods in which the impact of advective-diffusive mixing *on the shape* of the PDF is explicitly resolved (modeled). Thus our approach differs from all past PDF-based cloud physics schemes where the PDF shape is specified, *a priori*, to obey a specified analytic form. We further

demonstrate that our new PDF model is consistent with both EDC behavior and RH-front sharpening that increases strongly with increasing $\mathrm{D_a}$.

4a. *PDF equations and conditional averaging*

Conditional averaging only appears in equations for PDFs that have been spatially averaged or coarse-grained in some sense. As a pertinent example, consider the contribution of C&E to the evolution of droplet size distribution, $n(r)$, as written by Stevens et al. (1998):

$$\frac{\partial n(r,\boldsymbol{x},t)}{\partial t} = -\frac{\partial}{\partial r}\left[r^{1/3} n(r,\boldsymbol{x},t)\mathcal{L}(\boldsymbol{x},t)\right],$$

where $\mathcal{L}(\boldsymbol{x},t)$ is a single-valued scalar function. Stevens et al. (1998) apply a Reynolds decomposition to arrive at

$$\begin{aligned}\frac{\partial \langle n\rangle(r,\boldsymbol{x},t)}{\partial t} &= -\frac{\partial}{\partial r}\Big[r^{1/3}\langle n\rangle(r,\boldsymbol{x},t)\langle\mathcal{L}\rangle(\boldsymbol{x},t)+ \\ &\qquad r^{1/3}\left\langle n'(r,\boldsymbol{x},t)\mathcal{L}'(\boldsymbol{x},t)\right\rangle\Big], \qquad (9)\end{aligned}$$

where $\langle\cdot\rangle$ represents either ensemble averaging or spatial averaging centered at $\boldsymbol{x}$. The density $\langle n\rangle$ thus represents a "coarse-grained" PDF defined over a distribution of unresolved $\mathcal{L}'$ values.

To reveal the conditional average in Eq. (9) it is useful to introduce the field $\tilde{r}(\boldsymbol{x},t)$ distinct from the argument r of the density n. Substitution of the Dirac delta function, $\delta(r-\tilde{r}) \equiv n(r)$, clarifies the following algebraic manipulation:

$$\begin{aligned}\langle n'(r,\boldsymbol{x},t)\mathcal{L}'(\boldsymbol{x},t)\rangle &\equiv \langle[\delta\{r-\tilde{r}(\boldsymbol{x},t)\}-\langle n\rangle]\mathcal{L}'(\boldsymbol{x},t)\rangle \\ &= \frac{\langle\delta\{r-\tilde{r}(\boldsymbol{x},t)\}\mathcal{L}'(\boldsymbol{x},t)\rangle}{\langle\delta\{r-\tilde{r}(\boldsymbol{x},t)\}\rangle}\langle\delta\{r-\tilde{r}(\boldsymbol{x},t)\}\rangle \\ &\equiv \langle\mathcal{L}'(\boldsymbol{x},t)|r\rangle\langle n\rangle(\boldsymbol{x},t). \qquad (10)\end{aligned}$$

Eq. (10) is thus a restatement of Bayes' classic theorem. The conditional average $\langle\mathcal{L}'(\boldsymbol{x},t)|r\rangle$ appears on the rhs of Eq. (10) as the single unresolved quantity requiring parameterization.

With the preceding discussion in mind, we introduce the PDF equation for RH, in general form (Kilmenko and Bilger 1999, Eq. (41)):

$$\frac{\partial\mathcal{P}(\widetilde{\mathrm{RH}}=\mathrm{RH},t)}{\partial t} = -\frac{\partial}{\partial\mathrm{RH}}\left[\left\langle\frac{\partial\widetilde{\mathrm{RH}}}{\partial t}\middle|\widetilde{\mathrm{RH}}=\mathrm{RH}\right\rangle\mathcal{P}(\mathrm{RH},t)\right],$$

where $\widetilde{\mathrm{RH}}(\boldsymbol{x},t)$ is the spatio-temporal RH field, $\langle\cdot\rangle$ represents a subgrid spatial average and $\mathcal{P}(\mathrm{RH},t)$ is a spatially independent (averaged) density function with angular brackets dropped for notational convenience.

Substitution of Eq. (3) with no-flux boundary conditions gives

$$\begin{aligned}\left\langle\frac{\partial\widetilde{\mathrm{RH}}}{\partial t}\middle|\mathrm{RH}\right\rangle &= \kappa\left\langle\nabla^2\widetilde{\mathrm{RH}}|\mathrm{RH}\right\rangle \\ &\quad +4\pi D_v\left\langle\frac{Nr^2}{r+a}\middle|\mathrm{RH}\right\rangle(1-\mathrm{RH}), \qquad (11)\end{aligned}$$

where we have used $\langle\boldsymbol{u}\cdot\boldsymbol{\nabla}\widetilde{\mathrm{RH}}|\mathrm{RH}\rangle = 0$ (Kilmenko and Bilger 1999, Eq. (37)). Evaluation of these conditional averages is the subgrid modeling challenge for the RH-PDF with RH evolution given by Eq. (3).

4b. *Evaluation of conditional advection-diffusion*

Advective-diffusive mixing impacts $\mathcal{P}(\mathrm{RH})$ solely through the conditional Laplacian $\langle\nabla^2\widetilde{\mathrm{RH}}|\mathrm{RH}\rangle$—the RH Laplacian averaged on level-sets of RH. The conditional Laplacian has proved challenging to model. Evaluation using a Gaussian closure [also known as the linear mean-square estimation (LSME) model; see Larson (2004)] produces unsatisfactory behavior unless $\mathcal{P}$ is strictly Gaussian itself. While LSME and other models exhibit damping of scalar fluctuations, relaxation toward near-Gaussian statistics has proved difficult to capture.

In this series we evaluate $\langle\nabla^2\widetilde{\mathrm{RH}}|\mathrm{RH}\rangle$ using Chen et al. (1989)'s mapping closure. In this method, the single point statistics of $\widetilde{\mathrm{RH}}(\boldsymbol{x},t)$ are mapped to a time-independent Gaussian random field $\widetilde{\mathrm{RH}}_0(\boldsymbol{x})$ using a time-dependent mapping $\mathrm{RH} = X(\mathrm{RH}_0,t)$. Once X is established, $\mathcal{P}$ is given by

$$\mathcal{P}(\widetilde{\mathrm{RH}}=\mathrm{RH},t) = \mathcal{P}_0(\widetilde{\mathrm{RH}}_0=\mathrm{RH}_0)\left(\partial X/\partial\mathrm{RH}_0\right)^{-1}, \qquad (12)$$

where $\mathcal{P}_0$ denotes the single-point PDF of the centered Gaussian random field. Closure is achieved by assuming that the (unknown) spatial statistics of $\widetilde{\mathrm{RH}}$ are the same as the surrogate field $\widetilde{\mathrm{RH}}_0$. In particular, this implies

$$\langle\nabla^2\widetilde{\mathrm{RH}}|\mathrm{RH}\rangle = \langle\nabla^2\widetilde{\mathrm{RH}}_0|X(\mathrm{RH}_0)\rangle.$$

Using this approach, the evolution equation for X is an explicit function of the spatial statistics of the surrogate field. Chen et al. derive

$$\frac{\partial X}{\partial t} = \chi_0\left(-\frac{\mathrm{RH}_0}{\langle\widetilde{\mathrm{RH}}_0^2\rangle}\frac{\partial X}{\partial\mathrm{RH}_0}+\frac{\partial^2 X}{\partial\mathrm{RH}_0^2}\right)+Q(X), \qquad (13)$$

where $\chi_0 \equiv \kappa\langle|\boldsymbol{\nabla}\widetilde{\mathrm{RH}}_0|^2\rangle$, corresponding to the conditionally-averaged advection-diffusion equation, (11), with source term $Q(\widetilde{\mathrm{RH}})$. The final step in the derivation relates χ and χ_0, using either Gaussian relations (Chen et al. 1989) or direct evaluation of $\langle X^2\rangle$

in (13):

$$\chi = \chi_0 \left\langle (\partial X/\partial \mathrm{RH}_0)^2 \right\rangle .$$

Note that a complete closure requires independent specification of χ which we discuss in Sec. 4d.

Eq. (13) reveals the essential physics of X evolution. The first term on the rhs of (13) advects X away from $\mathrm{RH}_0 = 0$ toward both $+\infty$ and $-\infty$. In addition, diffusion smooths the features of X leading to near-Gaussian statistics via Eq. (13). This is the essential feature of mapping closure that assures physically reasonable behavior: anti-diffusional behavior in RH-space is translated into diffusional evolution in RH_0-space that is stable and mathematically well-defined. As shown by Gao (1991a,b), this RH_0-space evolution leads to a well-mixed state that is near-Gaussian but retains some memory of its initial non-Gaussian form, in good agreement with numerical experiment.

4c. *Evaluation of conditional C&E*

Continuing with the time-independent droplet radius assumption introduced in Sec. 3, Eq. (11) shows that $\langle N|\mathrm{RH}\rangle$ is the single conditional quantity required for C&E evaluation. Consider an analytic parameterization of $\langle N|\mathrm{RH}\rangle$ of the form

$$\langle N|\mathrm{RH}\rangle = F(t)\overline{N_c}\left(\frac{\mathrm{RH}-\mathrm{RH}_{\mathrm{env}}}{1-\mathrm{RH}_{\mathrm{env}}}\right)^{\beta}, \qquad (14)$$

for $\mathrm{RH}_{\mathrm{env}} \le \mathrm{RH} \le 1$ where $F(t)$ satisfies the normalization $\int \mathcal{P}(\mathrm{RH})\mathrm{dRH}\ \langle N|\mathrm{RH}\rangle = \langle N\rangle$. Eq. (14) states that *on average* the expected droplet concentration increases with increasing RH.

The exponent β in Eq. (14) controls the relative rate at which droplets "mix" into subsaturated regions of largely unmixed environmental air. In particular the limit $\beta \to \infty$ implies infinitely slow droplet mixing while $\beta \to 0$ implies infinitely quick mixing. The value $\beta = 1$ is an exact result for the given initial conditions in the absence of C&E, sedimentation and diffusive effects. Thus we expect β to be a function of Damköhler number and to approach unity as $\mathrm{D_a} \to 0$.

We employ the following strategy in determining $\beta(\mathrm{D_a})$. Firstly, we estimate the asymptotic scaling $\beta \sim {\mathrm{D_a}}^{1/2}$ as $\mathrm{D_a} \to \infty$ based on an analysis of $\mathrm{var}(\mathrm{RH})$ evolution predicted by mapping closure and Eq. (14). This analysis is presented in Appendix C. Secondly, we find that the relation

$$\beta = 1 + 0.015{\mathrm{D_a}}^{1/2}, \qquad (15)$$

is consistent with EDC and the results of Sec. 3c as shown in Sec. 4e.

4d. *Specification of* χ

PDF methods, including mapping closure, require independent specification of the scalar dissipation rate $\chi(t)$. Here we use a simple Newtonian damping term

$$\chi(t) = \mathrm{var}(\mathrm{RH})/\tau_{\mathrm{eddy}}, \qquad (16)$$

where a time-independent τ_{eddy} is specified a priori. Specification of a linear dependence of χ on $\mathrm{var}(\mathrm{RH})$ is frequently employed in cloud modeling studies and dates back to the early work of Mellor and Yamada (1974) and Wyngaard and Coté (1974), among others.

Combining Eqs. (13), (14) and (16) and introducing the non-dimensional time $\tau = t/\tau_{\mathrm{eddy}}$ gives

$$\frac{\partial X}{\partial \tau} = \frac{\langle X^2\rangle - \langle X\rangle^2}{\left\langle (\partial X/\partial \mathrm{RH}_0)^2 \right\rangle}\left(-\mathrm{RH}_0\frac{\partial X}{\partial \mathrm{RH}_0} + \frac{\partial^2 X}{\partial \mathrm{RH}_0^2}\right) + \mathrm{D_a}F(\tau)\left(\frac{X-\mathrm{RH}_{\mathrm{env}}}{1-\mathrm{RH}_{\mathrm{env}}}\right)^{\beta}(1-X), \qquad (17)$$

where $\langle\cdot\rangle$ represents an ensemble average over a normal distribution of RH_0 values with unit variance, and $F(\tau)$–computed numerically at each time step–satisfies $F(0) = 1$ and $F(\tau \to \infty) = (1 - \phi_{\mathrm{sub}})$ for the initial conditions used here. Eqs. (15), (17) and (5) complete the specification of our new PDF model of subgrid cloud mixing and evaporation.

4e. *Results*

PDF models lack explicit spatial information so they do not suffer from the usual numerical and computational issues associated with a diverging range of length scales that plague traditional 2D and 3D models. This advantage is illustrated by our new PDF approach which predicts (i) front propagation across the domain and associated evaporation limitation in agreement with EDC and (ii) increasing front sharpness with increasing $\mathrm{D_a}$. These phenomena are *easily resolved* in RH-probability-space (and numerically in $X(\mathrm{RH}_0)$-space) despite the fact that the front spatial structure is *unresolved*, and moreover, indeterminate.

In our PDF approach, good quantitative agreement between EDC and the present model is achieved, in part, by the tuning of β in Eq. (15). This is demonstrated in Fig. 6 which compares $\tau_{\mathrm{efold}}/\tau_{\mathrm{eddy}}$ predicted by the PDF model with the eddy-diffusivity model of Sec. 3c. The figure shows that both models predict τ_{efold} becoming independent of τ_{react} at large $\mathrm{D_a}$, in agreement with EDC phenomenology. However, it is important to emphasize that the EDC behavior demonstrated by the present PDF model is not merely a "tuned" phenomena. In fact, the boundary

conditions $\{N(\mathrm{RH_{env}}) = 0, N(1) = \overline{N_c}\}$ ensures that $\overline{N'\mathrm{RH}'} \neq 0$, and hence $\tau_{\mathrm{efold}} > \tau_{\mathrm{react}}$, for any reasonable interpolation of $N(\mathrm{RH})$ between these two endpoints.

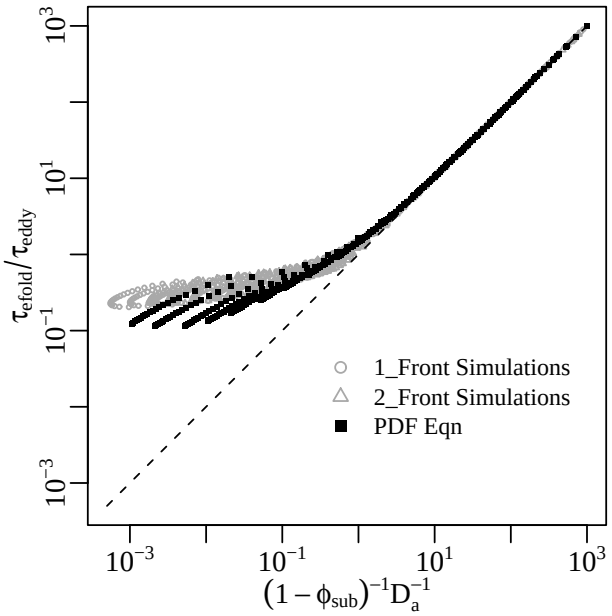

Figure 6: Comparison of $\tau_{\mathrm{eddy}}/\tau_{\mathrm{efold}}$ predicted by the 1_Front and 2_Front simulations of Sec. 3c, and the new PDF model of Sec. 4d. PDF simulations compute $X(\mathrm{RH}_0)$ using Eq. (17) such that $\overline{\mathrm{RH}}$ is an X-weighted average over a normal RH_0-distribution.

We now compare the present PDF model with the eddy-diffusivity model of Sec. 3c to compare and contrast consistency in $\overline{N'S'}$ and filament volume fraction predicted by these two very different approaches. A comparison of $\overline{\rho_2}$ vs $(1-\phi_{\mathrm{sub}})\mathrm{D_a}$ in Fig. 7(a) shows good agreement over the full range of $(1-\phi_{\mathrm{sub}})\mathrm{D_a}$ values, although a tendency of the PDF model to predict slight higher $\overline{\rho_2}$ values for $1 < (1-\phi_{\mathrm{sub}})^{-1}{\mathrm{D_a}}^{-1} < 10$ is noted.

However, large differences are seen in the filament volume fraction (CDF) predicted by the two approaches—a comparison shown in Fig. 7(b). In particular, the PDF approach predicts significantly smaller CDF values at large $\mathrm{D_a}$, indicative of RH-front sharpening. The observed differences can be interpreted as a Reynolds number effect: the eddy-diffusivity approach predicts a turbulent transport that is overly smooth at large times—with no cascade of variance to smaller scales—and hence at lower effective Reynolds number. However, Fig. 7(b) demonstrates that our new PDF approach—which does not suffer from spatial or numerical resolution limitations—does, in fact, capture an RH-front sharpening process that increases linearly with $\mathrm{D_a}$ to good approximation.

4f. *Summary*

A new PDF-based approach to subgrid cloud modeling is developed that appears to be a higher Reynolds number alternative to simple 1D eddy-diffusivity modeling. While both the PDF model of this section and the eddy-diffusivity model of Sec. 3c predict similar EDC-like behavior, our PDF approach does not explicitly suffer from spatial resolution errors associated with RH-front sharpening with increasing $\mathrm{D_a}$. Taking the PDF model as the superior model, the nature of cloud front propagation and evaporation in the constant droplet radius limit is thereby described by the following phenomenology:

(a) $\tau_{\mathrm{efold}} \sim \max(\tau_{\mathrm{eddy}}, \tau_{\mathrm{react}})$
(b) $\lim_{\mathrm{D_a}\to\infty} \overline{\rho_2} \to 1$
(c) $\lim_{\mathrm{D_a}\to\infty} \mathrm{CDF} \sim (1-\phi_{\mathrm{sub}})^{-1}{\mathrm{D_a}}^{-1} \sim \tau_{\mathrm{react}}/\tau_{\mathrm{eddy}}.$

We further reemphasize that (a) is a restatement of Magnussen and Hjertager's EDC model while (c) is in opposition to the Broadwell–Breidenthal picture of cloud mixing and evaporation. In the next section, we test (a), and hence the EDC model, using the Stevens et al. (1996) scenario of cloud front propagation.

5. A test of EDC: spurious cloud-edge supersaturations

We showed in Secs. 3 and 4 that LES/CRM models using the approximation $\tau_{\mathrm{react}}(\boldsymbol{x}, t) = \overline{\tau_{\mathrm{react}}}(t)$ underestimate τ_{efold} and therefore overestimate cloud front evaporation at large Damköhler numbers. Enhanced numerical prediction of C&E at cloud edges—and resulting instabilities—was first studied by Klaassen and Clark (1985). Subsequent work focused on the application of monotonic advection schemes to mitigate these instabilities (Grabowski 1989; Grabowski and Smolarkiewicz 1990; Grabowski and Clark 1991). But not until the study of Stevens et al. (1996), was a purely non-advective mechanism for spurious cloud-edge supersaturation exposed.

Stevens et al. consider the non-diffusive propagation of a cloud front across a 1D grid cell at constant velocity (U) as described by the triplet $\{\theta_l, q_t, r\}$. Following past studies they investigate the evolution of the corresponding grid-cell averaged quantities $\{\Theta_l, Q_t, R\}$ with one novel difference—Stevens

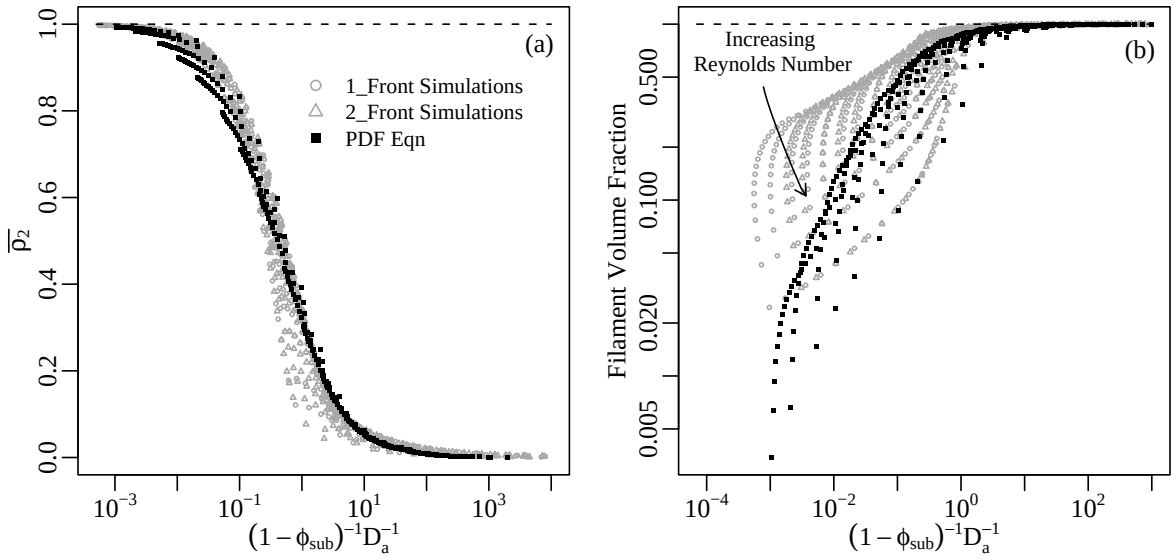

Figure 7: Comparison of the 1_Front and 2_Front simulations of Sec. 3c with the new PDF model of Sec. 4d. Fig. 7(a) shows the correlation coefficient, $\rho_2 = \overline{N'S'}/(\overline{N}\overline{|S|})$, averaged over $\tau_{\rm efold}$, while Fig. 7(b) shows the cumulative probability that $\mathrm{RH}_{\rm env} + \epsilon < \mathrm{RH} < 1 - \epsilon$, averaged over $\tau_{\rm efold}$ with $\epsilon = 0.01(1 - \mathrm{RH}_{\rm env})$. The eddy-diffusivity simulations—which appear to overestimate the CDF at large $\mathrm{D_a}$ in Fig. 7(b)—are, ostensibly, of lower effective Reynolds number than the corresponding PDF simulations.

et al. diagnose the grid-scale advective tendency without approximation, i.e. $U\nabla\Psi = \overline{U\nabla\psi}$ where the pair $\{\Psi, \psi\}$ is one of the three thermodynamic parameters. By assuming that advection can be performed perfectly at the grid-scale, the effect of subgrid modeling assumptions is, thereby, isolated. The Stevens et al. scenario, generalized to include turbulent eddy-diffusive mixing, provides an additional framework to study the effectiveness of the EDC model.

5a. *Modified Stevens et al. model*

Stevens et al. observe large fluctuations in $\overline{\mathrm{RH}}$ when C&E at the grid-scale is evaluated using $\{\Theta_l, Q_t, R\}$. As shown in their Fig. 3(b), supersaturations reach 4% and, quite counter-intuitively, supersaturation oscillations increase with *decreasing* τ where τ is the time required for the cloud front to propagate across the grid cell. Stevens et al. attribute these large fluctuations in S to the logical consequence of driving microphysical forcings with grid-averaged supersaturations. However, there is an additional forcing in their study that is causing S to exceed 1%, namely, the approximation $Q_l \sim R^3$ [their Eq. (4)] used in the calculation of T from $\Theta_l(Q_l)$. The exact advective tendencies of $\{Q_l, R\}$ are linear in time while the approximation $Q_l \sim R^3$ gives $Q_l \sim t^3$, an underestimation as seen in their Fig. 3(d). By underestimating the advective tendency of Q_l, Stevens et al. underestimate T [Fig. 3(a)] and overestimate RH [Fig. 3(b)], independent of C&E.

We consider evolution of the triplet $\{\Theta_l, Q_t, Q_l\}$ with advective tendencies evaluated exactly from $\{\theta, q_t, q_l\}$ such that the diagnosed advective tendency of T is linear in time.[†] In addition, we extend Stevens et al.'s laminar problem by adding eddy-diffusive mixing:

$$\frac{\partial \Psi}{\partial t} = -\overline{U\nabla\psi} + \kappa_e \overline{\nabla^2 \psi},$$

for $\Psi \in \{\Theta_l, Q_t\}$ where

$$\psi(x,t) = \Psi_e + \frac{(\Psi_c - \Psi_e)}{2}\mathrm{erfc}\left(\frac{x - Ut}{\sqrt{4\kappa_e t}}\right)$$

is the analytic solution for the evolution of a cloud-edge initialized at $(x = 0, t = 0)$, and Ψ_c (Ψ_e) represents unmixed cloud (clear) values.

In contrast, Q_l is evaluated numerically according to

$$\frac{\partial Q_l^{(n)}}{\partial t} = -\overline{U\nabla q_l} + \kappa_e \overline{\nabla^2 q_l} + \overline{\mathcal{F}}^{(n)}, \qquad (18)$$

[†]Note that $\exp\{-L_v Q_l/(c_{p,a}T)\} = 1 - L_v Q_l/(c_{p,a}T)$ to good approximation for the thermodynamic parameters used in Stevens et al. and here.

where $\overline{\mathcal{F}}^{(n)}, n \in \{1,2,3\}$ represents three different grid-scale microphysical forcings:

$$\begin{aligned}\overline{\mathcal{F}}^{(1)} &= \frac{\mathrm{d}Q_l}{\mathrm{d}t}\left\{R \sim Q_l^{1/3}\right\}\\ \overline{\mathcal{F}}^{(2)} &= \mathcal{L}\frac{\mathrm{d}Q_l}{\mathrm{d}t}\left\{R \sim Q_l^{1/3}\right\}\\ \overline{\mathcal{F}}^{(3)} &= \mathcal{L}\frac{\mathrm{d}Q_l}{\mathrm{d}t}\left\{R \sim Q_l^{1/3}(1-\phi_{\mathrm{sub}})^{2/3}\right\},\end{aligned}$$

and $\mathcal{L} = \tau_{\mathrm{react}}/\max(\tau_{\mathrm{eddy}}, \tau_{\mathrm{react}})$ when $\mathrm{d}Q_l/\mathrm{d}t < 0$ and 1 otherwise. Specifically, $\overline{\mathcal{F}}^{(1)}$ denotes the usual grid-scale averaged C&E-forcing with diagnostic relation $R \sim Q_l^{1/3}$ *overestimating* droplet radius, $\overline{\mathcal{F}}^{(2)}$ denotes the evaporation-limiting EDC model also with $R \sim Q_l^{1/3}$, and $\overline{\mathcal{F}}^{(3)}$ denotes the EDC model with improved diagnosis of R. Straightforward substitution verifies that the evaporation limiter, $\mathcal{L}$, produces EDC behaviour in the RH-equation that agrees with Eq. (8). We diagnose grid-cell cloud fraction crudely according to $\phi_{\mathrm{sub}}(t) = (\Psi_c - \Psi)/(\Psi_c - \Psi_e)$; this definition of ϕ_{sub} is exact for $\kappa_e = 0$, questionable otherwise. Explicit relations for $\mathrm{d}Q_l/\mathrm{d}t$ and τ_{react} are given in Appendix B.

In our implementation of the EDC model described above and in Appendix B, no attempt is made to "tune" the evaporation limitation via a constant of proportionality that relates τ_{efold} and τ_{eddy}, e.g. as per Eq. (8). Rather, our aim is to provide a first-order assessment of the efficacy of the EDC model in a mixing scenario that includes advection and cross-grid transport, and that is distinct from Sec. 3. Consistent with the treatment of advection-diffusion (above), the EDC model is applied at each time step with $\tau_{\mathrm{eddy}}(t) = \mathrm{var}(\mathrm{RH})/\chi$ calculated "exactly" from the fully-resolved subgrid field.

In Stevens et al. (1996)'s original scenario the single time-scale $\tau = L/U$ describes the purely advective transport across the grid cell; the addition of diffusion, here, introduces a second time-scale $\tau_\kappa = L^2/\kappa_e$. Since, our analysis continues to use τ as the primary time-scale we consider only $N_\kappa \leq 0.1$ where $N_\kappa \equiv \tau/\tau_\kappa$ is a non-dimensional measure of the relative importance of diffusion.

5b. *Results*

Plots comparing $\{\overline{\mathrm{RH}}, \overline{\mathrm{RH}}^{(1)}, \overline{\mathrm{RH}}^{(3)}\}$ and $\{\overline{q_l}, Q_l^{(1)}, Q_l^{(3)}\}$ as functions of t/τ for each $N_\kappa \in \{0, 0.01, 0.1\}$ are shown in Fig. 8. Before considering the impact of EDC on grid-averaged quantities, it is of interest to assess differences in $\overline{\mathrm{RH}}^{(1)}$ for $\kappa_e = 0$ between the present approach and Stevens et al., as seen in their Fig. 3(b). The grid-averaged supersaturation, $\overline{\mathrm{RH}}^{(1)} - 1$, gently plateaus near 0.2% in the current approach, while Fig. 3(b) in Stevens et al. shows a pronounced supersaturation peak that reaches 1.5%. As discussed in the previous subsection, the cause of the enhanced supersaturation oscillation in their work is the approximation $Q_l \sim R^3$ which causes grid-average temperatures to be underestimated. Consequently, $\overline{\mathrm{RH}}^{(1)}$ converges to $\overline{\mathrm{RH}}$ in the limit $\tau \to 0$ in the present approach but the opposite behavior is exhibited in Stevens et al.'s Fig. 3(b).

Fig. 8 also demonstrates the effect of the EDC model on grid-cell averaged quantities with R diagnosed from $Q_l^{1/3}(1-\phi_{\mathrm{sub}})^{2/3}$. Qualitatively, the agreement between $\{\overline{\mathrm{RH}}^{(3)}, Q_l^{(3)}\}$ and $\{\overline{\mathrm{RH}}, \overline{q_l}\}$ is very good. In particular, EDC limits the large evaporation rates that otherwise cause oscillations in the supersaturation field. In fact, for the original Stevens et al. scenario with $\kappa_e = 0$, the predictions of the EDC model are exactly correct. Essentially, this is a trivial limit of the EDC model in 1D where $\tau_{\mathrm{efold}} \to \infty$ as $\kappa_e \to 0$.

5c. *Statistics*

The ability of the EDC model to predict subgrid evaporation rates is quantified in Table 1 for $\tau \in \{32, 181, 1024\}$, $\overline{\mathcal{F}}^{(1-3)}$, and statistics averaged over τ. In addition to root-mean-square errors in grid-scale quantities $\overline{\mathrm{RH}}^{(n)}$ and $Q_l^{(n)}$, Table 1 presents $\overline{\mathrm{D_a}}^{(n)}$, the time-averaged Damköhler number, and $\theta_{\mathrm{lim}}^{(n)}$, the fraction of time that $\tau_{\mathrm{eddy}} > \tau_{\mathrm{react}}$ and evaporation rates are mitigated. These two statistics indicate that, for the majority of each grid-cell evolution, $\mathrm{D_a}$ is large and the grid-cell largely unmixed for $N_\kappa \leq 0.1$. In fact the large θ_{lim} values imply that the EDC-modeled evaporation rates for the present scenario are primarily determined by τ_{eddy}, independent of τ_{react}.

The standard deviations enumerated in Table 1 indicate that EDC, modeled using either $\overline{\mathcal{F}}^{(2)}$ or $\overline{\mathcal{F}}^{(3)}$, improves the prediction of grid-scale $\overline{\mathrm{RH}}$ and Q_l *without exception for the present parameter values*. For $\kappa_e \neq 0$, $\overline{\mathcal{F}}^{(3)}$ provides uniformly better estimates of subgrid evaporation than $\overline{\mathcal{F}}^{(2)}$.

The results of Table 1 are calculated with $\tau_{\mathrm{eddy}}(t)$ continuously diagnosed from the resolved subgrid field. This resolved subgrid information is, of course, not available in a typical LES/CRM model. In the spirit of Sec. 3, we consider two models that use a *single* τ_{eddy} value per simulation: (a) $\tau_{\mathrm{eddy}}(t) = \langle\tau_{\mathrm{eddy}}\rangle_\tau$ and (b) $\tau_{\mathrm{eddy}} = 0.05\tau/N_\kappa$ where $\langle\cdot\rangle_\tau$ represents a temporal average over e-folding time $e^{-1}\tau$. The coefficient 0.05 in (b) is selected (tuned) to produce good performance for the present scenario.

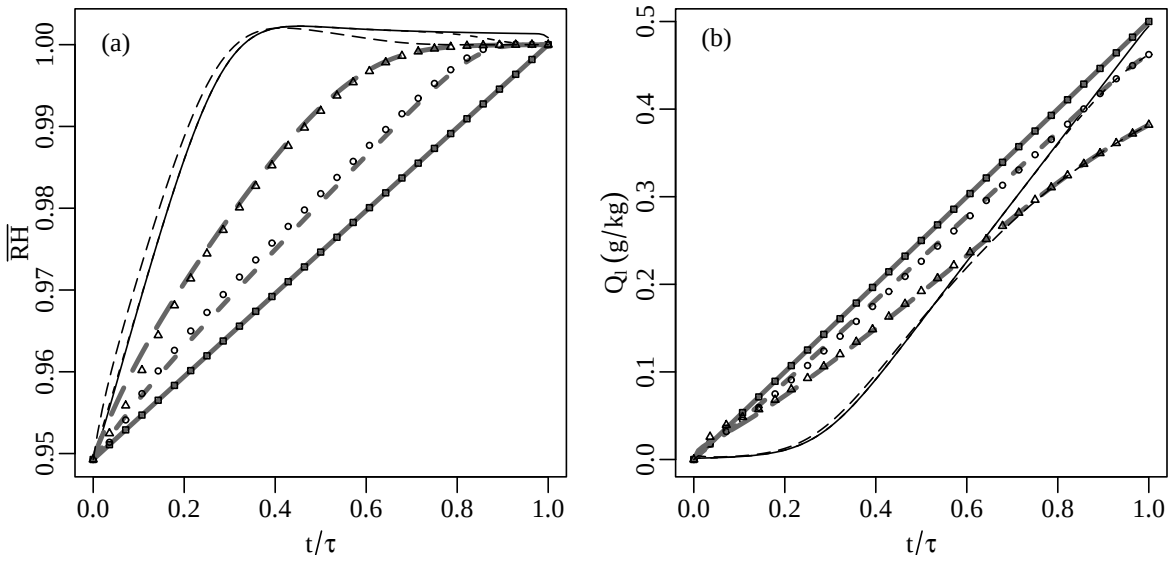

Figure 8: Comparison of $\overline{\mathrm{RH}}$ [Fig. 8(a)] and Q_l [Fig. 8(b)] diagnosed exactly from the resolved subgrid field (thick lines) and computed using grid-cell averaged microphysical forcing with evaporation limitation ($\overline{\mathcal{F}}^{(3)}$ in Eq. (18); symbols) and without ($\overline{\mathcal{F}}^{(1)}$ in Eq. (18); thin lines). Line and symbol types represent different N_κ values: {——,□} is $N_\kappa = 0$, {- - -,○} is $N_\kappa = 0.01$, and {– –,△} is $N_\kappa = 0.1$. Evaporation limitation based on the EDC model produces $\{\overline{\mathrm{RH}}, Q_l\}$ evolution that agrees closely with the resolved subgrid field. Calculations performed with $\tau = 181$ s and parameter value from Stevens et al. (1996, Table 1). Note that the thin solid line overlays the thin dashed line for $t < 0.8\tau$.

To demonstrate that the performance of EDC with $\tau_{\mathrm{eddy}}(t)$ described by (a) and (b) is comparable to Table 1, root-mean-square errors in $\overline{\mathrm{RH}}$ and Q_l are calculated over $\tau \in \{32, 181, 1024\}$, $N_\kappa \in \{0, 0.01, 0.1\}$ and listed in Table 2. Overall, the three different determinations of τ_{eddy} exhibit similar accuracy for the present scenario. And the sensitivity of all three parameterizations to $\overline{\mathcal{F}}^{(1-3)}$ is also similar: $\overline{\mathcal{F}}^{(1)} \rightarrow \overline{\mathcal{F}}^{(2)}$ improves performance by a factor of 2–4 and $\overline{\mathcal{F}}^{(2)} \rightarrow \overline{\mathcal{F}}^{(3)}$ improves performance by an additional factor of 1.5–2.

5d. *Summary*

Stevens et al. construct a novel scenario of purely advective cloud front propagation across a grid cell in 1D where spurious oscillations are observed in the grid-scale prognostic variables $\{\Theta_l, Q_t, R\}$. They do not suggest a solution to this problem.

We have shown that the EDC model exactly solves the non-turbulent problem articulated by Stevens et al.—and appears to provide good results for the more general turbulent case—with three important caveats:

- Stevens et al. use the approximation $Q_l \sim R^3$ in the determination of temperature which introduces a second grid-scale forcing that is independent of C&E. We avoid this forcing by using a different prognostic triplet, $\{\Theta_l, Q_t, Q_l\}$.

- The accuracy of EDC for $\kappa_e > 0$ depends, in turn, on the accuracy of the subgrid parametrization for τ_{eddy}. Good results using $\tau_{\mathrm{eddy}} = 0.05L^2/\kappa_e$ for the present scenario suggest that reasonably accurate diagnosis of τ_{eddy}, while difficult, is feasible.

- The surrogate problem for 3D turbulent transport tested here—advection and eddy-diffusion in 1D—is of limited complexity. In particular, incompressible advection is confined to a constant and trivial mean sweep in 1D. EDC has yet to be tested in 3D where advection plays a dominant role in cascading variance from large to small scales.

τ	N_κ	$\overline{\mathrm{D_a}}^{(2)}$	$\overline{\mathrm{D_a}}^{(3)}$	$\theta_{\mathrm{lim}}^{(1)}$	$\theta_{\mathrm{lim}}^{(2)}$	$\theta_{\mathrm{lim}}^{(3)}$	$\sigma_{\mathrm{RH}}^{(1)}$	$\sigma_{\mathrm{RH}}^{(2)}$	$\sigma_{\mathrm{RH}}^{(3)}$	$\sigma_{Q_l}^{(1)}$	$\sigma_{Q_l}^{(2)}$	$\sigma_{Q_l}^{(3)}$
32	0	∞	∞	0	1	1	1.8	0	0	0.062	0	0
	0.01	33.6	15.6	0	0.93	0.86	1.4	0.38	0.10	0.048	0.013	0.0036
	0.1	5.45	2.4	0	0.87	0.65	0.81	0.43	0.21	0.027	0.015	0.0072
181	0	∞	∞	0	1	1	2.2	0	0	0.072	0	0
	0.01	130	60	0	0.95	0.91	1.7	0.56	0.084	0.058	0.019	0.0027
	0.1	19.9	8.16	0	0.93	0.89	1.1	0.53	0.084	0.037	0.018	0.0028
1024	0	∞	∞	0	1	1	2.2	0	0	0.072	0	0
	0.01	589	275	0	0.94	0.92	1.8	0.67	0.36	0.059	0.023	0.012
	0.1	84.1	32.9	0	0.92	0.90	1.1	0.57	0.30	0.037	0.019	0.010

Table 1: Accuracy of the different microphysical forcings, $\overline{\mathcal{F}}^{(1-3)}$, for $\tau \in \{32, 181, 1024\}$ and $N_\kappa \in \{0, 0.01, 0.1\}$ as given by (i) $\sigma_{\mathrm{RH}}^{(1-3)}$—time-averaged standard deviation of RH (%), and (ii) $\sigma_{Q_l}^{(1-3)}$—deviation of Q_l (g/kg). The use of evaporation limitation in the source terms $\overline{\mathcal{F}}^{(2-3)}$ improves the prediction of $\{\overline{\mathrm{RH}}, Q_l\}$ in all cases. Also tabulated are (i) the time-averaged Damköhler number, $\overline{\mathrm{D_a}}^{(2-3)}$, where $\mathrm{D_a}(t) = \tau_{\mathrm{eddy}}{\tau_{\mathrm{react}}}^{-1}(1-\phi_{\mathrm{sub}})^{-1}$ with $\phi_{\mathrm{sub}}(t) = (\Psi_c - \Psi)/(\Psi_c - \Psi_e)$, and (ii) the fraction of time that the EDC model limits evaporation, $\theta_{\mathrm{lim}}^{(1-3)}$.

τ_{eddy}	$\overline{\mathrm{D_a}}^{(2)}/\overline{\mathrm{D_a}}^{(3)}$	$\theta_{\mathrm{lim}}^{(1)}$	$\theta_{\mathrm{lim}}^{(2)}$	$\theta_{\mathrm{lim}}^{(3)}$	$\sigma_{\mathrm{RH}}^{(1)}$	$\sigma_{\mathrm{RH}}^{(2)}$	$\sigma_{\mathrm{RH}}^{(3)}$	$\sigma_{Q_l}^{(1)}$	$\sigma_{Q_l}^{(2)}$	$\sigma_{Q_l}^{(3)}$
$\tau_{\mathrm{eddy}}(t)$	2.28	0	0.95	0.89	1.1	0.44	0.18	0.037	0.015	0.0060
$\langle\tau_{\mathrm{eddy}}\rangle_\tau$	2.99	0	1	0.93	1.1	0.20	0.14	0.037	0.0067	0.0046
$0.05\tau/N_\kappa$	2.98	0	0.99	0.93	1.1	0.28	0.17	0.037	0.0094	0.0059

Table 2: Comparison of the accuracy of three different methods for calculating τ_{eddy}: (i) $\tau_{\mathrm{eddy}}(t) = \mathrm{var}(\mathrm{RH})/\chi$ calculated without approximation at each time-step from the resolved subgrid field, (ii) $\tau_{\mathrm{eddy}} = \langle\tau_{\mathrm{eddy}}(t)\rangle_\tau$ calculated a priori as an average over e-folding time $e^{-1}\tau$, and (iii) diagnostic relation $\tau_{\mathrm{eddy}} = 0.05\tau/N_\kappa$. All three methods exhibit similar accuracies. Standard deviation are averaged over $\tau \in \{32, 181, 1024\}$ and $N_\kappa \in \{0, 0.01, 0.1\}$.

6. Summary

Prediction of the turbulent evolution of a mixture of clear and cloudy air is, fundamentally, a Lagrangian problem that is of higher dimension than that of typical reactive scalar systems. The interaction of a droplet with the surrounding temperature and vapor fields depends, in particular, on the droplet radius which is expressed as a Lagrangian path integral along droplet trajectories. This reveals an essential difficulty in predicting droplet spectral evolution—and hence evaporation—at unresolved scales.

In this work we exploit a time-independent droplet radius approximation—appropriate for $\mathrm{RH}_t > 1$, large drops and small subsaturations—that essentially removes the Lagrangian character from the problem at hand. In particular, this assumption implies that cloud front propagation and evaporation is independent of the specifics of the droplet size distribution and a function of only two time-scales, τ_{react} and τ_{eddy}. Two common cloud schemes (i) PDF schemes that exploit the InC&E assumption and (ii) LES/CRM schemes that resolve τ_{react} and ignore subgrid correlations make diametric assumptions $\tau_{\mathrm{efold}} \sim \tau_{\mathrm{eddy}}$ and $\tau_{\mathrm{efold}} \sim \tau_{\mathrm{react}}$, respectively. We refer to these relations as the C&E time-scale dilemma: two common subgrid cloud modeling assumptions, that are in some sense archetypal, are inherently inconsistent.

The resolution to the C&E time-scale dilemma is found in the pioneering work of Magnussen and Hjertager (1976) who first hypothesized the relation $\tau_{\mathrm{efold}} \sim \max(\tau_{\mathrm{eddy}}, \tau_{\mathrm{react}})$ which encapsulates the behavior of traditional PDF and resolved C&E schemes at different limits. We have verified using two very different conceptual approaches—1D eddy-diffusivity modeling and a new PDF approach with resolved C&E—that Magnussen and Hjertager's EDC model correctly predicts the evaporation rate for cloud-front propagation across a grid-cell in the constant radius limit and in the absence of sedimentation and inertial effects. These results imply that PDF schemes overestimate evaporation at small Damköhler number while LES/CRM models that resolve C&E overestimate evaporation at large $\mathrm{D_a}$.

Although the estimate $\mathrm{D_a} \sim L^{2/3}$ might suggest that PDF and LES/CRM schemes are correct in typical small and large grid size limits, respectively, Fig. 1 demonstrates otherwise. For example, at 20 m res-

olution, the LES/CRM approximation $\tau_{\rm efold} \sim \tau_{\rm react}$ becomes invalid at r greater than about 50 μm and $\overline{N_c} = 50$ cm^{-3}; at $\overline{N_c} = 500$ cm^{-3} the LES/CRM approximation breaks down near 5 μm. In a similar fashion, PDF schemes that utilize the InC&E assumption are not uniformly valid at $L = 1000$ m and typical atmospheric conditions. These results reiterate and substantiate concerns that have been raised in the cloud physics literature that modeled evaporation rates are too high (Krueger 1993; Stevens et al. 1996), or more generally, are of particular importance to overall model performance (Stevens et al. 2005).

Implementation of the EDC model in high-resolution schemes requires modifying the C&E source term for $\mathrm{d}q_l/\mathrm{d}t$ with the evaporation limiter $\mathcal{L} = \tau_{\rm react}/\max(c_1\tau_{\rm eddy}, \tau_{\rm react})$ when $\mathrm{d}q_l/\mathrm{d}t < 0$; direct substitution verifies that $\mathcal{L}$ correctly reproduces the EDC behavior $\tau_{\rm efold} \sim \max(\tau_{\rm eddy}, \tau_{\rm react})$ in the RH-equation and constant radius limit. Our numerical simulations suggest $c_1 \approx 0.35$. This new scheme additionally requires the diagnosis of (subgrid) $\tau_{\rm eddy}$ from the resolved field. We have tested this implementation of EDC with diagnostic relation $\tau_{\rm eddy} = c_2 L^2/\kappa_e$ in a turbulent generalization of the Stevens et al. (1996) scenario of 1D cloud front propagation and find very good quantitative results for $c_2 = \mathcal{O}(0.1)$. This result is encouraging because L and κ_e are already standard computed quantities in many LES/CRM models. We plan to test the efficacy of this implementation of EDC in 2D simulations of a non-precipitating cumulus in the near future using the HIGRAD cloud model (Reisner et al. 2001, 2005).

The present work introduces a new PDF-based approach for modeling cloud mixing and evolution that is distinct from other PDF cloud schemes in three important ways: (i) turbulent mixing and C&E are explicitly resolved, i.e. the InC&E assumption is relaxed, (ii) the PDF shape is not specified a priori, and (iii) the model reproduces EDC behavior in quantitative agreement with 1D eddy-diffusivity simulations. Analysis of the volume fraction of filaments containing a mixture of clear and cloudy air suggests that the present PDF approach is, effectively, a higher Reynolds number simulation than the corresponding eddy-diffusivity simulations.

Although our new model of the RH-PDF, $\mathcal{P}(\mathrm{RH})$, plays an important but supporting role in this article it provides new information that will be further investigated in subsequent articles in this series. As an illustrative example, a plot of the evolution of $\mathcal{P}(\mathrm{RH})$ calculated at $\mathrm{D_a} = 100$ is shown in Fig. 9. The figure reveals that our new PDF approach successfully resolves *in probability space* the extremely small volume-fraction filaments where mixing is occurring—a feature that has proved difficult to capture in Eulerian spatial models. Together with the parameterization for $\langle N|\mathrm{RH}\rangle$, Eq. (14), $\mathcal{P}(\mathrm{RH})$ provides the distribution of subsaturations experienced by a population of droplets. Thus, in principle, our PDF approach allows for the complete evaporation of some drops while others remain unchanged; this is the "inhomogeneous mixing" process of Baker et al. (1980). However, further progress in this direction requires the development of a Lagrangian droplet model that lives in RH-probability space and which removes the constant droplet radius assumption employed in this study. This line of investigation is currently being pursued.

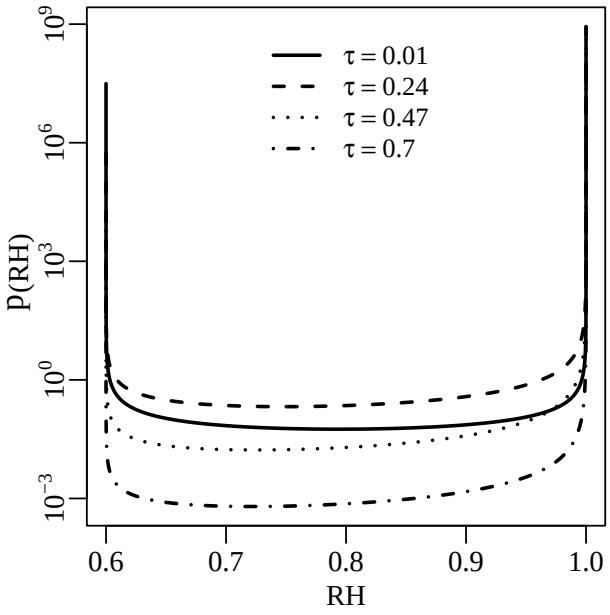

Figure 9: Plot of RH-PDF evolution calculated using Eq. (12) and the present PDF model with $\mathrm{D_a} = 100$, $\mathrm{RH_{env}} = 0.6$ and $\phi_{\rm sub} = 0.5$. Four snapshots are shown for $\tau \in \{0.01, 0.24, 0.47, 0.7\}$ where $\tau = t/\tau_{\rm eddy}$. At $\tau = 0.7$ very little of the pure environmental air is left although this is masked in the figure by the overlap of lines at $\mathrm{RH} = \mathrm{RH_{env}}$.

Acknowledgement This work was funded by a Los Alamos National Laboratory Directed Research and Development Project entitled "Resolving the Aerosol-Climate-Water Puzzle (20050014DR)". We thank Nicole Jeffery and Manvendra Dubey for their comments on this manuscript.

A. The InC&E assumption and cloud evaporation

The analog of Eqs. (6) for subgrid PDF schemes that use the InC&E assumption is

$$\begin{aligned} \frac{\partial \mathrm{RH}_t}{\partial t} &= \kappa_e \nabla^2 \mathrm{RH}_t \\ \mathrm{RH} &= \min(1, \mathrm{RH}_t), \end{aligned} \tag{19}$$

with $\overline{ql} \sim \overline{\Gamma(\mathrm{RH}_t - 1)(\mathrm{RH}_t - 1)}$ where Γ is a step function. To generate the shaded regions in Fig. 2, Eqs. (19) are first solved using 1_Front and 2_Front initial conditions for $\Delta\overline{ql} \in [0.01, 0.30]\overline{ql}$ and a distribution of ϕ_{sub}. The range of τ_{efold} shown in Fig. 2 is then calculated by averaging over ϕ_{sub}.

B. Microphysical relations for Sec. 5

Let

$$\frac{\mathrm{d}Q_l}{\mathrm{d}t} = 4\pi \frac{\rho_w}{\rho_a} \overline{N_c} \mathcal{R}^2 \frac{\mathrm{d}\mathcal{R}}{\mathrm{d}t},$$

with

$$\begin{aligned} \frac{\mathrm{d}\mathcal{R}}{\mathrm{d}t} &= c_r Q_s \frac{\rho_a}{\rho_w} D_v \frac{\overline{\mathrm{RH}} - 1}{\mathcal{R} + a} \\ c_r &= \left\{ 1 + \frac{D_v}{D_a} \left(\frac{L_v}{R_v T} - 1 \right) \frac{L_v}{c_{p,a} T} Q_s \right\}^{-1}, \end{aligned}$$

and parameter values $\overline{N_c} = 100\,\mathrm{cm}^{-3}$, $a = 2\ \mu\mathrm{m}$, and thermodynamics parameters as in standard texts (Pruppacher and Klett 1997).

Then the diagnosis of $\mathcal{R}$ in $\overline{\mathcal{F}}^{(1-3)}$ obeys

$$\begin{aligned} \overline{\mathcal{F}}^{(1-2)} &\rightarrow \mathcal{R} = R \\ \overline{\mathcal{F}}^{(3)} &\rightarrow \mathcal{R} = R(1 - \phi_{\mathrm{sub}})^{2/3}, \end{aligned}$$

with

$$R = \left(\frac{3}{4\pi} \frac{\rho_a}{\rho_w} \frac{Q_l}{\overline{N_c}} \right)^{1/3},$$

and

$$\tau_{\mathrm{react}} = \frac{1}{4\pi D_v \overline{N_c}} \frac{\mathcal{R} + a}{\mathcal{R}^2}.$$

C. Determination of β

A prediction for the $\mathrm{D_a}$ dependence of β follows from consideration of the behavior of the first two moment of RH as predicted by the evolution of the map, X. Combining Eqs. (11), (13) and (14) gives

$$\begin{aligned} \frac{\partial \langle \mathrm{RH}^n \rangle}{\partial \tau} &= -2\chi\tau_{\mathrm{eddy}}\delta_{n,2} + \int_{-\infty}^{\infty} \mathcal{P}_0(\mathrm{RH}_0)\mathrm{dRH}_0\ nF(t) \\ &\quad \mathrm{D_a} \left(\frac{X - \mathrm{RH_{env}}}{1 - \mathrm{RH_{env}}} \right)^{\beta} X^{n-1}(1 - X), \end{aligned} \tag{20}$$

with $n \in \{1, 2\}$. We can gain insight into the dynamics of Eq. (20) by considering the production and dissipation of variance implied by the approximate exponential traveling wave solution:

$$X(\mathrm{RH}_0) = \begin{cases} c_1 \exp\left[\lambda(\mathrm{RH}_0 - vt)\right] + \mathrm{RH_{env}} & \mathrm{RH}_0 < vt \\ 1 & \text{otherwise} \end{cases}$$

with $c_1 = (1 - \mathrm{RH_{env}})$ and $v < 0$. Assuming $\beta \gg 1$ and $\lambda \gg 1$ such that $\mathcal{P}_0(\mathrm{RH}_0)$ is a constant in Eq. (20) gives

$$\frac{\partial \mathrm{var(RH)}}{\partial \tau} = -2\chi\tau_{\mathrm{eddy}} + 2\mathrm{D_a}\mathcal{P}_0(vt)F(t)\frac{(1 - \mathrm{RH_{env}})^2}{\lambda\beta^2}(1 - \overline{\mathrm{RH}}). \tag{21}$$

The two terms on the rhs of Eq. (21) represent the impact of eddy-diffusion and evaporation on $\mathrm{var(RH)}$ as the cloud-front propagates across the domain. The EDC model and the results of Sec. 3 indicate that evolution of $\mathrm{var(RH)}$ should become independent of $\mathrm{D_a}$ as $\mathrm{D_a} \rightarrow \infty$ for the unmixed initial conditions considered here. Along with Eq. (21), this implies the scaling $\beta \sim {\mathrm{D_a}}^{1/2}$.

References

Baker, M. B., R. G. Corbin, and J. Latham, 1980: The influence of entrainment on the evolution of cloud droplet spectra: I. A model of inhomogeneous mixing. *Q. J. R. Meteorol. Soc.*, **106**, 581–599.

Bilger, R. W., 1976: The structure of diffusion flames. *Combust. Sci. and Tech.*, **13**, 155–170.

Broadwell, J. E. and R. E. Breidenthal, 1982: A simple model of mixing and chemical reaction in a turbulent shear layer. *J. Fluid Mech.*, **125**, 397–410.

Chen, H., S. Chen, and R. H. Kraichnan, 1989: Probability distribution of a stochastically advected scalar field. *Phys. Rev. Lett.*, **63**, 2657–2660.

Cooper, W. A., 1989: Effects of variable droplet growth histories on droplet size distributions. Part I: Theory. *J. Atmos. Sci.*, **46**, 1301–1311.

Damköhler, G. Z., 1940: Influence of turbulence on flame velocity in gaseous mixtures. *ZH Electrochem*, **46**, 601.

Gao, F., 1991a: An analytical solution for the scalar probability density function in homogeneous turbulence. *Phys. Fluids*, **A3**, 511–513.

— 1991b: Mapping closure and non-gaussianity of the scalar probability density functions in isotropic turbulence. *Phys. Fluids*, **A3**, 2438–2444.

Grabowski, W. W., 1989: Numerical experiments on the dynamics of the cloud-environment interface: Small cumulus in a shear-free environment. *J. Atmos. Sci.*, **46**, 3513–3541.

— 1993: Cumulus entrainment, fine-scale mixing, and buoyancy reversal. *Q. J. R. Meteorol. Soc.*, **119**, 935–956.

Grabowski, W. W. and T. L. Clark, 1991: Cloud-environment interface stability: Rising thermal calculations in two spatial dimensions. *J. Atmos. Sci.*, **48**, 527–546.

Grabowski, W. W. and P. K. Smolarkiewicz, 1990: Monotone finite-difference approximations to the advection-condensation problem. *Mon. Wea. Rev.*, **118**, 2082–2097.

Heymsfield, A. J. and G. M. McFarquhar, 2001: Microphysics of INDOEX clean and polluted trade cumulus clouds. *J. Geophys. Res.*, **106**, 28653–28673.

Jeffery, C. A. and P. H. Austin, 2003: Unified treatment of thermodynamic and optical variability in a simple model of unresolved low clouds. *J. Atmos. Sci.*, **60**, 1621–1631.

Kilmenko, A. Y. and R. W. Bilger, 1999: Conditional moment closure for turbulent combustion. *Prog. Energy Comb. Sci.*, **25**, 595–687.

Klaassen, G. P. and T. L. Clark, 1985: Dynamics of the cloud-environment interface and entrainment in small cumuli: Two-dimensional simulations in the absence of ambient shear. *J. Atmos. Sci.*, **42**, 2621–2642.

Krueger, S. K., 1993: Linear eddy modeling of entrainment and mixing in Stratus clouds. *J. Atmos. Sci.*, **50**, 3078–3090.

Larson, V. E., 2004: Prognostic equations for cloud fraction and liquid water, and their relation to filtered density functions. *J. Atmos. Sci.*, **61**, 338–351.

Lohmann, U. and J. Feichter, 2005: Global indirect aerosol effects: a review. *Atmos. Chem. Phys.*, **5**, 715–737.

Magnussen, B. F. and B. H. Hjertager, 1976: On mathematical modeling of turbulent combustion with special emphasis on soot formation and combustion. *Sixteenth Symposium (International) on Combustion*, Pittsburgh, Pa : Combustion Institute, Cambridge, MA, USA, 719–729.

— 1979: Calculation of flow, mixing, and evaporation of a two-phase mixture injected into a hot gas stream. *Two-phase Momentum, Heat and Mass Transfer in Chem, Process, and Energy Eng Syst*, Washington, DC : Hemisphere Publ Co, Dubrovnik, Yugosl, 411–422.

Majda, A. and P. Souganidis, 2000: The effect of turbulence on mixing in prototype reaction-diffusion systems. *Comm. Pure Appl. Math.*, **53**, 1284–1304.

Mellor, G. L., 1977: The Gaussian cloud model relations. *J. Atmos. Sci.*, **34**, 356–358, see also CORRIGENDA, **34**, 1483.

Mellor, G. L. and T. Yamada, 1974: A hierarchy of turbulence closure models for planetary boundary layers. *J. Atmos. Sci.*, **31**, 1791–1806.

Pruppacher, H. R. and J. D. Klett, 1997: *Microphysics of Clouds and Precipitation*. Kluwer Academic, Boston, MA, USA, 2nd edition.

Reisner, J., V. Mousseau, and D. Knoll, 2001: Application of the newton-krylov method to geophysical flows. *Mon. Wea. Rev.*, **129**, 2404–2415.

Reisner, J. M., V. A. Mousseau, A. A. Wyszogrodzki, and D. A. Knoll, 2005: An implicitly balanced hurricane model with physics-based preconditioning. *Mon. Wea. Rev.*, **133**, 1003–1022.

Sommeria, G. and J. W. Deardorff, 1977: Subgrid-scale condensation in models of nonprecipitating clouds. *J. Atmos. Sci.*, **34**, 344–355.

Spalding, D. B., 1971: Mixing and chemical reaction in steady confined turbulent flames. *Thirteenth Symposium (International) on Combustion*, Pittsburgh, Pa : Combustion Institute, 649–657.

Squires, P., 1952: The growth of cloud drops by condensation. 1. General characteristics. *Aust. J. Sci. Res.*, **A5**, 59–86.

Stephens, G. L., 2005: Cloud feedbacks in the climate system: A critical review. *J. Climate*, **18**, 237–273.

Stevens, B., W. R. Cotton, and G. Feingold, 1998: A critique of one- and two-dimensional models of

boundary layer clouds with a binned representations of drop microphysics. *Atmos. Res.*, **47-48**, 529–553.

Stevens, B., C.-H. Moeng, A. S. Ackerman, C. S. Bretherton, A. Chlond, S. De Rhoode, and J. Edwards, 2005: Evaluation of large-eddy simulations via observations of nocturnal marine stratocumulus. *Mon. Wea. Rev.*, **133**, 1443–1462.

Stevens, B., R. L. Walko, and W. R. Cotton, 1996: The spurious production of cloud-edge supersaturations by Eulerian models. *Mon. Wea. Rev.*, **124**, 1034–1041.

Tennekes, H. and J. L. Lumley, 1972: *A First Course in Turbulence*. MIT Press, Cambridge, Massachusetts and London, England.

Wang, S., Q. Wang, and G. Feingold, 2003: Turbulence, condensation, and liquid water transport in numerically simulated nonprecipitating Stratocumulus clouds. *J. Atmos. Sci.*, **60**, 262–278.

Wyngaard, J. C. and O. R. Coté, 1974: The evolution of a convective planetary boundary-layer—a higher-order-closure model study. *Bound. Layer Meteor.*, **7**, 289–308.